Journal of Hydrology 619 (2023) 129328

Contents lists available at ScienceDirect

Journal of Hydrology

journal homepage: www.elsevier.com/locate/jhydrol

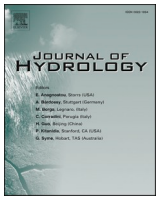

Research papers

Bridging the gap from hydrological to biogeochemical processes using tracer-aided hydrological models in a tropical montane ecosystem

Juan Pesántez [a,*], Christian Birkel [b], Giovanny M. Mosquera [c], Rolando Célleri [a], Pablo Contreras [a], Irene Cárdenas [a], Patricio Crespo [a]

[a] Departamento de Recursos Hídricos y Ciencias Ambientales & Facultad de Ingeniería, Universidad de Cuenca, Av. 12 de Abril, Cuenca, Ecuador
[b] Department of Geography and Water and Global Change Observatory, University of Costa Rica, 2060 San José, Costa Rica
[c] Instituto Biósfera, Universidad San Francisco de Quito USFQ, Quito, Ecuador

ARTICLE INFO

This manuscript was handled by S Sally Elizabeth Thompson, Editor-in-Chief

Keywords:
Stable isotopes
Andes
Storage
Transit times
Páramo
Tracers
DOC

ABSTRACT

How simple or complex catchment models need to be is still unclear particularly for tracer-aided models that go beyond hydrograph fitting. Here, we take advantage of a sub-daily hydrometric and tracer data set from a tropical montane (páramo) experimental catchment to fill this knowledge gap. We evaluated six conceptual rainfall-runoff model structures with different complexity that represent the perceptual understanding of the catchment's hydrological functioning. The models solved conservative and reactive tracer mass balances to simulate streamflow, stable isotopes, and DOC concentrations and were assessed for performance and parsimony using three calibration targets (discharge only, discharge and stable isotopes, and discharge and DOC), resulting in 18 model configurations. Although all models satisfied the discharge calibration (KGE $>$ 0.8), differences arose when considering tracer transport. The more complex models outperformed the simpler ones in terms of goodness-of-fit and parsimony, indicating that the catchment streamflow response consisted of quick near-surface flow and tracer contributions, more mixed flow through the two main soil types (Andosols and Histosols), as well as flow from the well-mixed shallow fractured rock (up to 20 m depth). The bedrock flow pathway contributed up to ~25% of total flow during baseflow conditions. This study provides a benchmark experiment to identify hydrological and biogeochemical behavior in tropical montane catchments using relatively parsimonious tracer-aided hydrological models.

1. Introduction

Montane catchments play a vital role in the water supply for millions of people (Messerli et al., 2004; Viviroli et al., 2007). An example is the vastly populated tropical Andes, which highly depends on flow generated from a tropical alpine ecosystem known as páramo (Buytaert et al., 2006a). Water provision from the páramo is essential not only to satisfy human demands, but also for irrigation, and hydropower generation (Celleri and Feyen, 2009). To date, some studies have focused on understanding and identifying environmental changes (e.g., climate change) and how they will affect these catchments (Bradley et al., 2006; Correa et al., 2020; Mora et al., 2014). Land use change driven by population growth, for example, is projected to intensify agricultural use, grazing, fire, and fertilization among others (Ochoa-Tocachi et al., 2016; Quichimbo et al., 2012). These activities could play a critical role in the transformation of páramo soils (e.g., by promoting tillage, increasing soil compaction, impairing hydrological buffering capacity), resulting in severe consequences for the hydrological and biogeochemical processes of the ecosystem (Patiño et al., 2021). In addition, climate change may lead to shifts in precipitation patterns and extremes, as well as increasing temperatures, particularly in the highest areas of the Andes (Bradley et al., 2006; Mora et al., 2014; Vuille, 2013). However, climate change impacts are still difficult to predict due to a limited understanding about the hydrological and biogeochemical functioning of paramo catchments (e.g.: water and solute mixing, transit times, and biogeochemical cycling) (Aparecido et al., 2017; Correa et al., 2020; Gutiérrez-Salazar and Medrano-Vizcaíno, 2019).

Rainfall-runoff modelling is amongst the most important tools to understand catchment hydrological behavior (Beven, 2012). Hydrological models assisted by conservative and reactive tracer information can provide a more comprehensive understanding of hydrological functioning (Buytaert and Beven, 2011; Clark et al., 2011; McGuire and

* Corresponding author.
E-mail address: juanp.pesantezv@ucuenca.edu.ec (J. Pesántez).

https://doi.org/10.1016/j.jhydrol.2023.129328
Received 13 October 2022; Received in revised form 23 February 2023; Accepted 26 February 2023
Available online 3 March 2023

McDonnell, 2015), and also to associated biogeochemical processes (Birkel and Soulsby, 2016; Dick et al., 2015; Regier et al., 2016). However, since models are simplifications of complex real-world systems with many inherent uncertainties, a thorough assessment as to how simple or complex they should be to adequately represent ecosystem processes is necessary (Beven and Chappell, 2021). In this sense, several authors have proposed to use models with different degrees of complexity and using them as multiple working hypotheses to identify the most appropriate and parsimonious model structure for a particular hydrological system (Buytaert and Beven, 2011; Clark et al., 2011; Pfister and Kirchner, 2017). In the following we refer to this as a multi-model framework.

The main goal within a multi-model framework is to identify the best-performing and most parsimonious model representation of the system, thus avoiding over- simplification and overparameterization of complex processes (Clark et al., 2011; Pfister and Kirchner, 2017). The multi-model framework has been used to answer scientific questions in the past; e.g., how to adequately evaluate major hydrological challenges in catchment modelling (e.g., model complexity, water fluxes, spatial variability, computational efficiency)? (Clark et al., 2015, 2017), how different model structures affect runoff simulations for climate change scenarios? (Dams et al., 2015; Reinecke et al., 2021), and how to improve the simulation of discharge and hydrological extremes by including human activity in hydrological models? (Veldkamp et al., 2018).

Although it is still not very common, including tracers within a multi-model framework could support an adequate simulation of flow paths and also the determination of the sources and residence times of water within a catchment (Birkel et al., 2014; Birkel and Soulsby, 2016; Hrachowitz et al., 2013; Mcdonnell and Beven, 2014; McMillan et al., 2012). In addition to a better understanding of catchment flow pathways, mixing, storage, and transit times, including biogeochemical processes, such as dissolved organic carbon (DOC) cycling in models, could represent a significant step towards bridging the gap between water quantity and quality. Hrachowitz et al. (2016) proposed transit time distributions (TTD) as the missing link between water quantity and quality, but tracer-aided hydrological models that accommodate the biogeochemical processes in their structure have the potential to provide important insights into water and nutrient cycling relations as well (Birkel et al., 2020). In high-elevation Andean catchments, transit times have been evaluated assuming steady state conditions and during baseflow conditions, not taking into account flow paths under variable wetness catchment conditions (Larco et al., 2023; Lazo et al., 2019; Mosquera et al., 2016b). In this context, the use of a tracer-aided multi-model framework can help to unveil interactions between hydrological and biogeochemical processes (Birkel et al., 2014). Few studies have incorporated tracers into a multi-model framework and we are not aware of any other study in the high-elevation tropics with similar objectives.

Understanding DOC dynamics is vital for supporting human and aquatic ecosystem health. High-temporal frequency in-stream DOC monitoring is relatively easy to achieve (Birkel et al., 2020; Chow et al., 2003; DeForest et al., 2018; Ouyang et al., 2006; Pesántez et al., 2021) and is particularly useful in peat-dominated ecosystems or those with carbon-rich soils such as the páramo because the high carbon content could result in the release of high amounts of DOC to the streams (Arízaga-Idrovo et al., 2022; Freeman et al., 2001). Moreover, if DOC dynamics are influenced by soil moisture and/or temperature, climate and land use change can significantly increase carbon release to streams (Pesántez et al., 2018; Vuille et al., 2000). Improved knowledge on DOC export sources and dynamics can help close the net carbon balance and enhance understanding of terrestrial-aquatic carbon connectivity in the páramo (Carrillo-Rojas et al., 2019).

Using a novel high-resolution flow and tracer data set (stable isotopes: 4- to 6-hours sampling; DOC: hourly sampling), we aimed to improve knowledge of hydrological and biogeochemical catchment functioning of the Andean páramo using a multi-model framework. Our specific aims were:

(1) to develop conceptual tracer-aided hydrological models of varying complexity to represent different empirically known hydrological processes for a data-rich tropical alpine (páramo) catchment,
(2) to identify the best model, representing catchment hydrological processes at a minimum complexity, by evaluating the performances of the models developed in (1), and,
(3) to link catchment hydrological behavior to biogeochemical processes through the simultaneous calibration of water fluxes and in-stream stable isotopes and DOC concentrations using tracer-aided hydrological models developed in (1).

2. Study site and current understanding of hydrological processes

The tropical alpine Zhurucay Ecohydrological Observatory (Table 1) is located on the western slope of the Andean Mountain range in the highlands of southern Ecuador (3°04′S, 79°14′W), and drains to the Pacific Ocean, at elevations between 3662 and 3900 m a.s.l. The observatory has been the focus of various hydrometeorological and ecohydrological studies aimed to enhance our understanding of rainfall-runoff processes in páramo catchments (Correa et al., 2017; Lazo et al., 2019; Mosquera et al., 2015; Mosquera et al., 2016a). These studies identified the Amazon rainforest situated east of the Andean mountain range as the main moisture source (Esquivel-Hernández et al., 2018; Zhiña et al., 2022) that generates mainly low-intensity precipitation throughout the year (Padrón et al., 2015) (Fig. 2).

Zhurucay is an energy-limited and water abundant system. It has two dominant landscape units that differ markedly in hydrological functioning: hillslopes and valley-bottom wetlands. The hillslopes are characterized by volcanic ash soils known as Andosols with tussock grass vegetation and cover 78 % of the catchment area. The valley-bottom wetlands are mainly composed of organic-rich, peat-type soils known as Histosols and cover 22 % of the catchment (Lazo et al., 2019; Mosquera et al., 2015). These wetlands are generally recharged by the hillslope Andosols. The wetlands close to the stream network significantly influence the water yield in Zhurucay. The chemical composition of the soils is composed of high contents of aluminum, iron, and other metals (Buytaert et al., 2005; Buytaert et al., 2006b). Another important feature is the high subsurface hydrological connectivity between hillslopes (Andosols) and wetlands (Histosols) during rainstorm events (Correa et al., 2019). Andosols have a lower saturated hydraulic conductivity (47 % less), and porosity (16 % less), than the shallow organic soil layers of the Histosols (Lazo et al., 2019; Mosquera et al., 2016a). Vertical soil water movement is driven by a quicker response of a shallow “organic soil horizon”, compared to the slower response of deeper soil layers (Table 1) (Crespo et al., 2012; Lazo et al., 2019; Mosquera et al., 2016a; Mosquera et al., 2021). The main runoff generation process is therefore the shallow subsurface flow in Histosols and Andosols. These differences in the páramo soils properties and distribution within the catchment affect the transport of water from the hillslopes (streams and soils) to the wetlands and therefore the regulation of water quantity and quality downstream.

Generally, rainfall that infiltrates the soil on the upper to the middle slope (Andosols) flows laterally through the shallow organic soil (Mosquera et al., 2016b). As it reaches the bottom of the slope (Histosols), more vertical flow paths are activated and the water reaches more hydrologically inactive zones in the wetlands (Mosquera et al., 2016a). Hortonian overland flow in these soils is rare due to the high porosity, infiltration capacity, and hydraulic conductivity of the soils, which is higher than typical rainfall intensities (Table 1). Observations indicate that Histosols remain close to saturation year-round; saturation is reached during periods of sustained rainfall or high-intensity rainfall

Table 1
Main features of the study catchment within the Zhurucay Ecohydrological observatory in the tropical alpine (páramo) highlands of southern Ecuador. For the mean values the standard deviation (±) or (range) is given in parentheses.

Parameter	Description	Units
Area of the studied sub catchment within the observatory	3.28	km^2
Study period	October 2017-February 2019	
Location	3°4'S, 79°14'W	
Elevation range	3676–3900	m a.s.l.
Average slope	18 (range: 0–46)	%
Climate [a]	Mainly from the Amazon Forest – Köppen-Geiger clasification: Cfc	–
Total precipitation during study period	1628	mm
Total discharge during study period	713	mm
Total actual ET during study period (based on Eddy covariance measures)[b]	821	mm
Mean temperature during study period	6.5 (±2.17)	°C
Min temperature during study period	2.4	°C
Max temperature during study period	15	°C
Mean relative humidity during study period	90 (±13.5)	%
Mean isotopic composition (d^2H)		
Precipitation	−70.0 (±34.8)	‰
Discharge	− 72.7 (±7.2)	‰
Mean DOC concentration in discharge	5.56 (±2.43)	$mg*L^{-1}$
Geology [c, d]	Quimsacocha = 50 Quaternary Deposits = 20 Turi = 30	%
Lithology [c, d]	Basaltic flows of plagioclases, feldspars, andesitic pyroclastic Miocene	–
Andosol soil cover (tussock grass veg.)	78	%
Hydraulic conductivity [e, f]	Andic horizon (Ah) ~ 8.2;Mineral horizon (C) ~ 5	mm h^{-1}
Bulk density [e, f]	Andic horizon (Ah) ~ 0.42; Mineral horizon (C) ~ 1.25	gr cm^{-3}
Mean organic matter content of soil [e, g]	29	%
Histosol soil cover (cushion plants veg.)	22	%
Hydraulic conductivity [e, f]	Organic horizon (O) ~ 15.5; Mineral horizon (C) ~ 7	mm h^{-1}
Bulk density [e, f]	Organic horizon (O) ~ 0.14Mineral horizon (C) ~ 0.91	gr cm^{-3}
Mean organic matter content of soil [e, g]	49	%

References: [a]Zhiña et al. (2022); [b]Carrillo-Rojas et al. (2019); [c]Beate, (1999); [d]Mosquera et al. (2015); [e]Quichimbo et al. (2012); [f]Mosquera et al. (2016b) and Correa et al. (2017); [g]Buytaert et al. (2005); Buytaert et al. (2006b). (–) Units not applicable.

events (Correa et al., 2019; Mosquera et al., 2016a).

Springs sourced by shallow groundwater also contribute to streamflow. The geology in Zhurucay is mainly composed by compacted volcanic rocks from the Quimsacocha (basaltic flows with plagioclases, feldspars, and andesitic pyroclasts), and Turi (tuffaceous andesitic breccias, conglomerates, and horizontal stratified sands) formations (Coltorti and Ollier, 2000). Hydrogeological surveys near Zhurucay revealed a shallow fractured rock layer of around 20 m depth (ITASCA DENVER Inc., 2020). This layer is hydraulically disconnected from the deeper bedrock which has a very low ("quasi-compact") permeability. Therefore, low deep groundwater contributions to streams were observed at Zhurucay traveling through mineral soil, especially during low flow conditions (Correa et al., 2017).

Transit times have been calculated in this ecosystem (~188 days) using lumped convolution integral models (Lazo et al., 2019; Mosquera et al., 2016b).

3. Materials and methods

3.1. Hydrometric data collection

Rainfall (P), streamflow (Q), and actual evapotranspiration (ET_a) were measured at 5-min resolution during the period October 2017-February 2019 (Fig. 2). A Texas Electronics tipping-bucket rain gauge (0.1 mm resolution, TR-525M, Dallas, TX, USA) was installed at the meteorological station, and two additional Onset rain gauges (0.2 mm resolution, RG3-M Onset, Bourne, USA) elsewhere in the catchment (Fig. 1). Both gauges have a 1% accuracy and were used to calculate the average precipitation in the catchment using the Thiessen polygon method. We installed CS616 water content reflectometers (Campbell Scientific, Logan, USA) next to the meteorological station at 10 cm soil depth to record soil water content (SWC). The SWC was recorded at a 5-min resolution and has a precision better than 0.1% with the calibration procedure explained in Ochoa-Sánchez et al., 2018. An INW (AquiStar CT2X, Kirkland, WA, USA) pressure transducer sensor with ± 0.06% accuracy was installed in a combined rectangular-V-notch weir at the micro-catchment outlet (Fig. 1) and used to measure the stream water level, which was transformed into discharge using a calibrated rating curve (percentage absolute error = 2.1%) (Guallpa et al., 2022), based on the Kindsvater-Shen equation (United States Bureau of Reclamation, 2001). Discharge was measured using the salt dilution technique (~17) (Guallpa et al., 2022). The calibration range (0.001–600 $l*s^{-1}$) was smaller than the observed discharge range (0.002–3093 $l*s^{-1}$) but the percentage of the time that the discharge was outside the calibration period was very small (0.9%). Actual evapotranspiration (ET_a: Fig. 2) was measured using the eddy covariance (EC) technique as explained in Carrillo-Rojaset al. (2019).

3.2. Tracer monitoring and water sampling

Two tracers were monitored during the period October 2017-February 2019: stable isotopes, specifically deuterium (δ^2H), and DOC (Fig. 2). Rain water for isotopic analysis was accumulated in a custom-made, pressure-based sequential rainfall sampler (Mcdonnell et al., 1990), collecting one sample for every 2.08 mm of rain (the setup of the device is described in detail in Zhiña et al., 2022). Streamflow samples were taken using a Campbell Scientific automatic sampler (PVS4100D, Logan, UT, USA) every four hours. Isotope laboratory analysis were carried out with a cavity ring-down spectrometer L2130-i Picarro (Picarro Inc., USA); the complete analysis procedure is explained in Zhiña et al., 2022. Even though both stable isotopes, oxygen-18 and deuterium (δ^2H) were analyzed, we used deuterium for illustration purposes (high values range) and refer to it as stable isotopes. The rainfall and streamflow samples plotted close to the global meteoric water line (Fig. 2-f), suggesting little to no evaporative fractionation. Therefore, both isotopes would yield identical results as tracers in modelling.

Streamflow DOC concentrations were estimated using an UV–Vis spectrometer (Spectrolyser, s::can Messtechnik GmbH,Vienna, Austria) following the calibration procedure described in detail in Pesántez et al. (2021) (number of samples used for calibration: 1822, normalized RMSE ~ 20%, Nash–Sutcliffe efficiency ~ 0.7, calibration range: 2–16 $mg*L^{-1}$ which was the same period and range as the present study, percentage of the time outside the calibration period: 0%)..

3.3. Tracer-aided multi-model conceptualizations

We formulated six different model structures based on previous

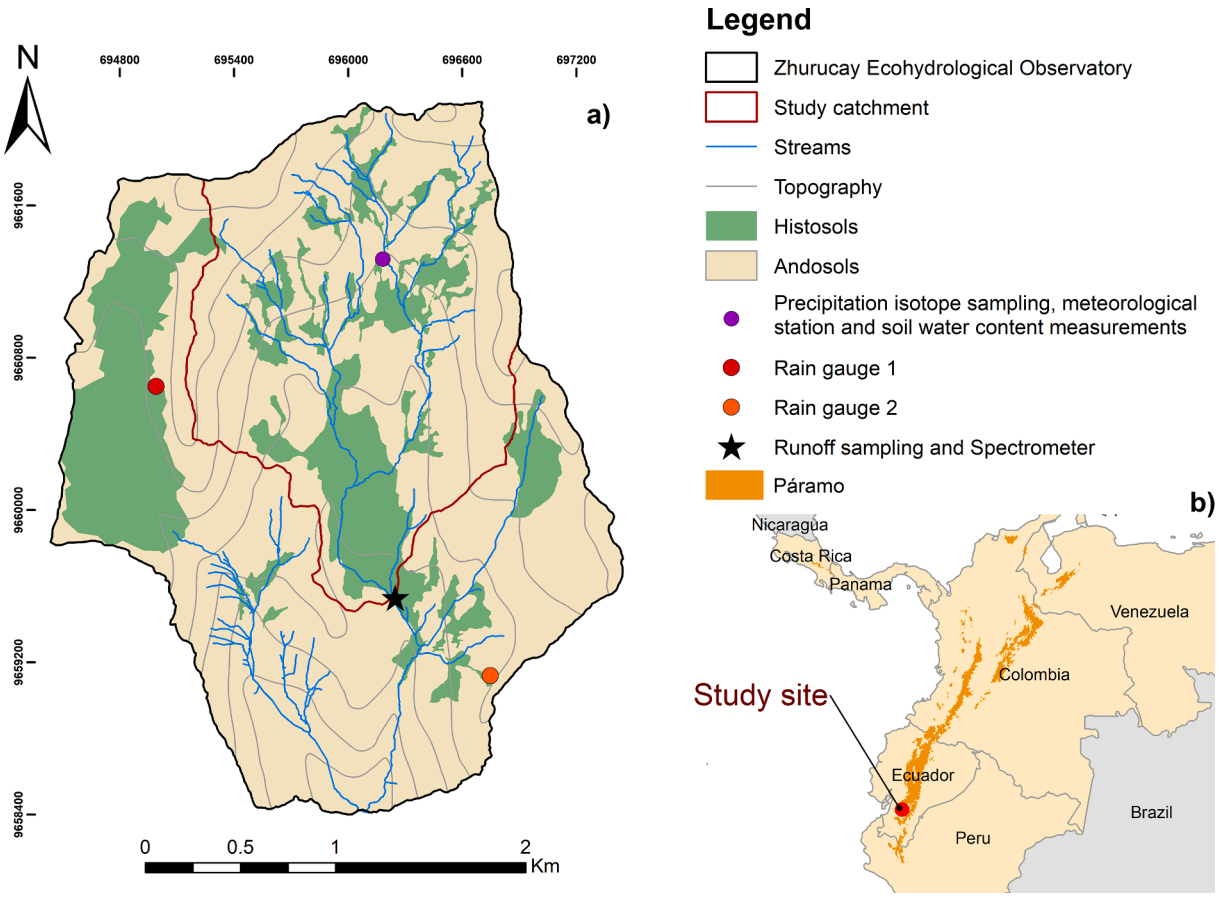

Fig. 1. a) Catchment map including the precipitation monitoring sites (meteorological station, rain gauge 1 and 2), streamflow gauging site (includes doc and stable isotopes sampling), and the meteorological station which includes an eddy covariance tower. b) The study catchment in the regional context of the latin-american tropical páramo ecosystem according to Correa et al. (2021).

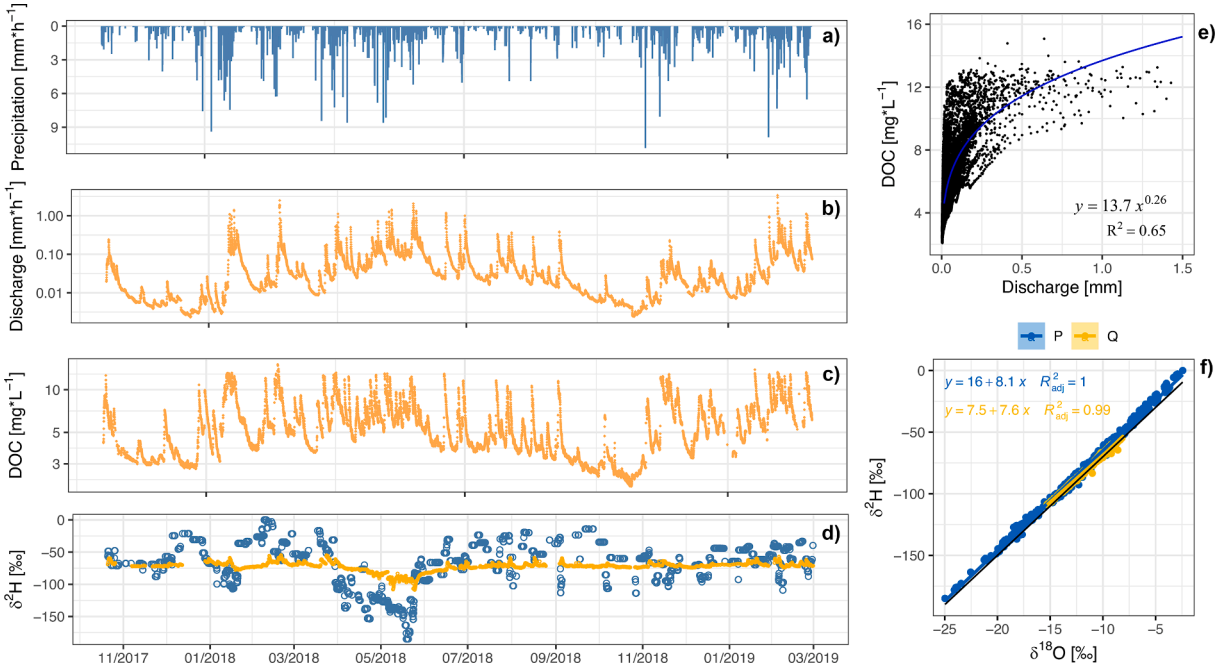

Fig. 2. Time series of hourly a) precipitation, b) discharge (Q), c) DOC concentrations, d) stable isotopes during events (blue) and every 4–6 h in streamflow (yellow), e) scatter plot of discharge Q vs DOC concentrations, and f) local meteoric water line (blue) and stream samples (yellow), compared to the GMWL (black line). (For interpretation of the references to colour in this figure legend, the reader is referred to the web version of this article.)

empirical understanding of páramo catchment hydrological behavior (Fig. 3). The model structures ranged from a simple lumped to a more complex semi-distributed structures and describe the role of the two dominant soil types or hydrologic response units for runoff (Fig. 3 and Table 2 for the model constitutive equations):

- Model M1 (Fig. 3-1) represents the simplest lumped conceptualization of two vertically connected reservoirs representing the soil profile: the shallow near surface reservoir generates relatively quick near-surface flow (Q_S), and is connected vertically to the deeper reservoir representing subsurface flow. The first shallow near surface

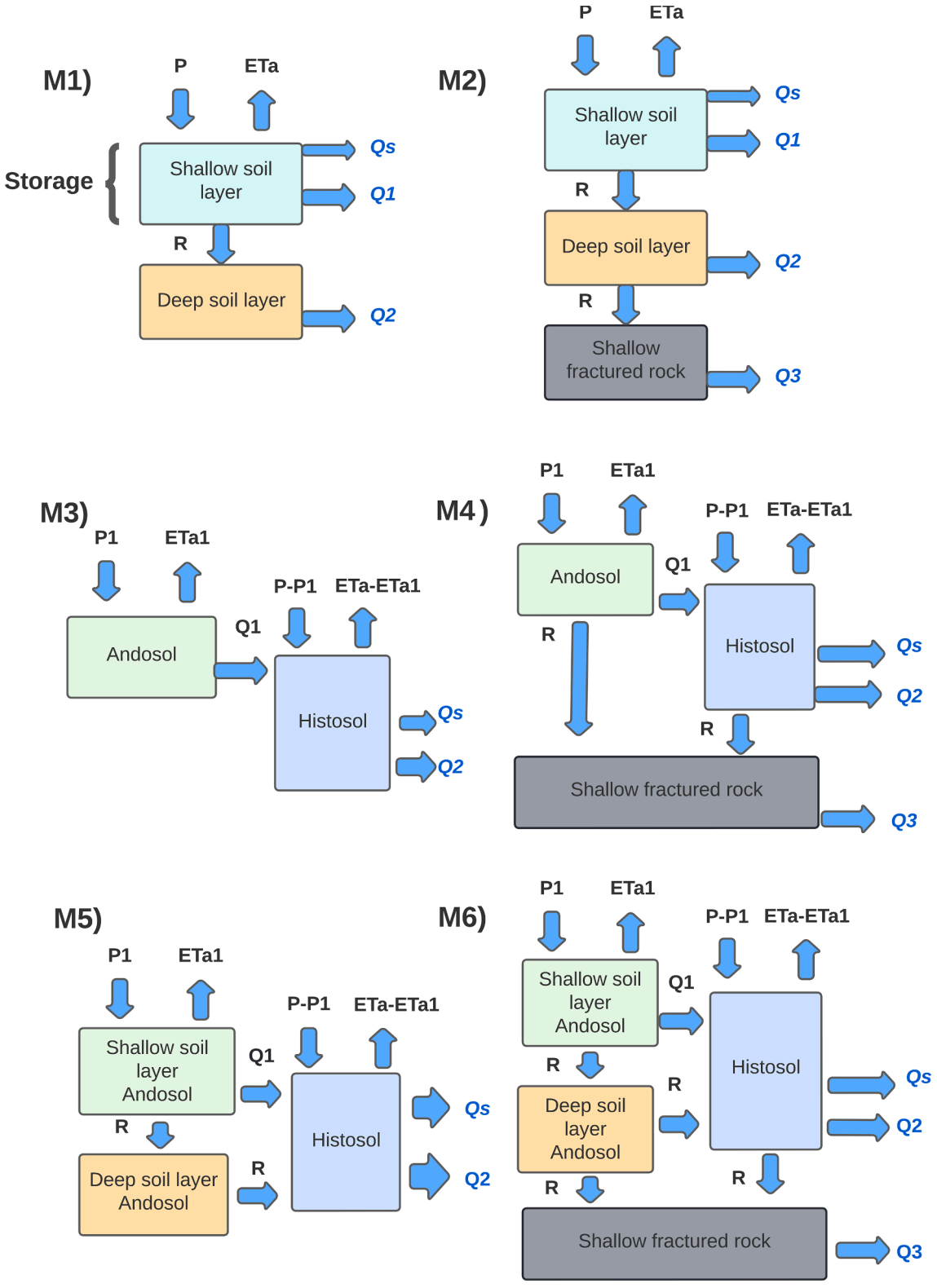

Fig. 3. Conceptual diagrams of the multi-model framework used in this study. Internal flow components are shown with black labels and all the model components that add up to total flow with blue labels. P: precipitation; ET_a: actual evapotranspiration; R: recharge; Q1- Q3: water flows from soils; Q_s: quick near-surface flow. (For interpretation of the references to colour in this figure legend, the reader is referred to the web version of this article.)

Table 2
Transfer functions used in the hydrological module and parameters used in the hydrological and tracer modules of the multi-model framework used in this study. Q represents flow that contributes to the stream, R represents the flux from one reservoir to another, S represents the storage in each reservoir, PS represents passive storage volume available for stable isotopes mixing, L represents DOC loss parameter. The reservoirs are in subscripts: shallow horizon reservoir (up), deep horizon reservoir (dw), Histosol reservoir (H), fractured rock reservoir (fr).

	Reservoir	Flux	Hydrological transfer functions	Parameters		
				Hydrological module	Stable isotopes module	Biogeochemical or DOC module
M1	Shallow soil	Stream	$Q_{up} = a{*}S_{up}^{1+\propto}$	a, ∝		
		Recharge	$R_{up} = r{*}(S_{up} - Q_{up})$	r	PS_{up}	k_{DOC}, E, L_{up}
	Deep soil	Stream	$Q_{dw} = b{*}S_{dw}$	b	PS_{dw}	L_{dw}
			Total number of parameters	4	6	8
M2	Shallow soil	Stream	$Q_{up} = a{*}S_{up}^{1+\propto}$	a, ∝		
		Recharge	$R_{up} = r{*}(S_{up} - Q_{up})$	r	PS_{up}	k_{DOC}, E, L_{dw}
	Deep soil	Stream	$Q_{dw} = b{*}S_{dw}$	b	PS_{dw}	L_{dw}
		Recharge	$R_{dw} = r_{dw}{*}(S_{dw} - Q_{dw})$	r_{dw}		
	Shallow fractured rock	Stream	$Q_{fr} = b_{fr}{*}Sfr$	b_{fr}	PS_{fr}	L_{fr}
			Total number of parameters	6	9	11
M3	Andosol	Stream	$Q_{up} = a{*}S_{up}^{1+\propto}$	a, ∝	PS_{up}	k_{DOC}, E, L_{up}
	Histosol	Stream	$Q_H = a_H{*}S_H^{1+\propto_H}$	a_H, $\propto_H$	PS_{dw}	k_{DOC}, E, L_H
			Total number of parameters	4	6	10
M4	Andosol	Stream	$Q_{up} = a{*}S_{up}^{1+\propto}$	a, ∝		
		Recharge	$R_{up} = r{*}(S_{up} - Q_{up})$	r	PS_{up}	k_{DOC}, E, L_{up}
	Histosol	Stream	$Q_H = a_H{*}S_H^{1+\propto_H}$	a_H, $\propto_H$		
		Recharge	$R_H = r_H{*}(S_H - Q_H)$	r_H	PS_H	k_{DOC}, E, L_H
	Shallow fractured rock	Stream	$Q_{fr} = b_{fr}{*}S_{fr}$	b_{fr}	PS_{fr}	L_{fr}
			Total number of parameters	7	10	14
M5	Shallow soil	Stream	$Q_{up} = a{*}S_{up}^{1+\propto}$	a, ∝		
		Recharge	$R_{up} = r{*}(S_{up} - Q_{up})$	r	PS_{up}	k_{DOC}, E, L_{up}
	Deep soil	Stream	$Q_{dw} = b{*}S_{dw}$	b	PS_{dw}	L_{dw}
	Histosol	Stream	$Q_H = a_H{*}S_H^{1+\propto_H}$	a_H, $\propto_H$	PS_H	k_{DOC}, E, L_{up}
			Total number of parameters	6	9	13
M6	Shallow soil	Stream	$Q_{up} = a{*}S_{up}^{1+\propto}$	a, ∝		
		Recharge	$R_{up} = r{*}(S_{up} - Q_{up})$	r	PS_{up}	k_{DOC}, E, L_{up}
	Deep soil	Stream	$Q_{dw} = b{*}S_{dw}$	b		
		Recharge	$R_{dw} = r_{dw}{*}(S_{dw} - Q_{dw})$	r_{dw}	PS_{dw}	L_{dw}
	Histosol	Stream	$Q_H = a_H{*}S_H^{1+\propto_H}$	a_H, $\propto_H$	PS_H	k_{DOC}, E, L_H
		Recharge	$R_H = r_H{*}(S_H - Q_H)$	r_H		
	Shallow fractured rock	Stream	$Q_{fr} = b_{fr}{*}S_{fr}$	b_{fr}	PS_{fr}	L_{fr}
			Total number of parameters	9	13	17

reservoir provides a quick, potentially preferential, response to the stream (Q_1). The shallow reservoir recharges the deeper (mineral) reservoir only if there is water available above field capacity. The deeper reservoir provides baseflow (Q_2) to the stream based on the linear reservoir assumption.

- Model M2 (Fig. 3-1) is similar to model M1, but additionally includes a shallow fractured rock reservoir that is recharged and drained in the same way as the mineral reservoir described for model 1(Q3).
- Model M3 (Fig. 3-3) is a semi-distributed conceptualization of two parallel reservoirs, which in this study represent the main soil types in the páramo ecosystem (Andosols on the hillslopes and Histosols in the valley bottoms connected to the stream). Both reservoirs can provide a quick preferential response to the stream, similar to the organic layers previously described. The water drains from the Andosol reservoir to the Histosol (Q_1) and then directly drains to the stream (Q_2). The Histosol reservoir generates quick near-surface flow (Q_S).
- Model M4 (Fig. 3-4) is similar to model M3 but includes a shallow fractured rock reservoir that is recharged by both, the Histosol (wetland) and Andosol (hillslopes) reservoirs. Only the Histosol (Q_2) and the shallow fractured rock (Q_3) reservoirs generate streamflow.
- Model M5 (Fig. 3-5) is a mix of models M1 and M3. Here, the Andosol consists of an organic (fast response) reservoir and a slower responding deeper reservoir, similar to the first structure. However, both hillslope reservoirs drain into the parallel Histosol reservoir, from which streamflow is generated (Q_2), representing a potentially faster response due to higher connectivity.
- Model M6 (Fig. 3-6) is similar to model M5, but additionally includes a fourth shallow fractured rock reservoir that is recharged by both the mineral reservoir of the Andosol and the Histosol reservoir. The Histosol quickly drains water to the stream (Q_2) plus the slower and more constant deeper baseflow contribution to streamflow from the deep reservoir (Q_3). The Histosol reservoir generates quick near-surface flow (Q_S).

Tracer mass balances for stable isotopes and DOC transport were implemented in the rainfall-runoff models. For these simulations, we used the dynamic storage volumes in the hydrological module to mix tracers in the reservoirs for the stable isotopes and to simulate the DOC dynamics in the biogeochemical module (Table 2). For the stable isotope module, we assumed a complete mixing of incoming rain with stored soil water isotopes. The complete mixing assumption was based on previous studies in the same catchment, that yielded the best results for the

paramo system (Lazo et al., 2019; Mosquera et al., 2016b). We also included calibrated passive storage volumes (PS_{up}: storage in the shallow soil water, PS_{dw}: storage in the deep soil water, and PS_{fr}: storage in shallow fractured rock) in each reservoir, creating additional volume for stable isotopes mixing and transport without affecting the dynamic storage in the hydrological module, similar to Birkel and Soulsby (2016). We define the term passive storage as the immobile or non-active water in the catchment (pore water or water that is outside the hydro-physical structure of the soil that has been observed through experimentation) and available for tracer mixing, but that does not hydrologically contribute to streamflow (Birkel et al., 2011).

The biogeochemical module used a production parameter (k_{DOC}, biogeochemical module: Table 2), an energy activation parameter (E), a simple loss parameter (L) that consumes, absorbs, or mineralizes DOC, and a calibrated soil moisture parameter that represents a lower limit to DOC production, similar to Birkel et al. (2017). We did not use air/soil temperature as a driver of DOC, because in tropical páramo ecosystems the temperature has a very low intra-annual variability (Córdova et al., 2016). Furthermore, Pesántez et al., 2018 identified soil moisture as the sole hydro-meteorological DOC control for natural páramo vegetation.

3.4. Model calibration and assessment

All models were calibrated using three different targets: i) only water fluxes (i.e., only calibrating Q), ii) water flux and stable isotopes (i.e., calibrating Q + stable isotopes), and iii) water flux and DOC (i.e., calibrating Q + DOC). For cases ii) and iii), tracer dynamics were simulated within the hydrological model and the hydrological and tracer modules were calibrated simultaneously. We split the data set in two parts: the first 75% was used for model calibration (October 2017–October 2018), and the other 25% for model validation (November 2018–February 2019). We applied a multi-objective genetic algorithm (NSGA2) (Deb et al., 2002) to simultaneously optimize the simulation of discharge (Q) and either tracer (stable isotopes and DOC). The two-dimensional, and equally weighted, optimized objective functions were:

i) the Kling-Gupta efficiency (KGE) of Q and the Nash-Sutcliffe efficiency (NSE) of Q,
ii) the KGE of Q and the KGE of stable isotopes, and
iii) the KGE of Q and the KGE of DOC.

The KGE accounts for correlation (r), bias (α), and variability (β). Expected KGE values range from $-\infty$ to 1 (NSE has the same range), with a value of 1 indicating a perfect fit (Gupta et al., 2009). Efficiencies above 0.45 were considered acceptable (Mosquera et al., 2016b). The NSGA2 seeks to minimize the objective functions and we therefore used 1 – KGE and 1 – NSE for model calibration and evaluation, i.e., values close to 0 indicate better model performance.

We used a total of 500 generations in each calibration run with 200 parameter set populations (Deb et al., 2002; Wang et al., 2019) to sufficiently explore the parameter space (100,000 iterations) for the different model configurations (4 to 18 calibrated parameters) (Table 2). We then retained the final (i.e., best) 200 solutions for each model to visualize simulation ranges as a qualitative indicator of parameter uncertainty. Two-dimensional Pareto fronts were used to visualize the resulting approximations found by the NSGA2 in terms of convergence, spread, and distribution of objective functions (Zitzler et al., 2003). Pareto fronts of each model and each calibration target were compared to assess model performance. In addition, the Bayesian Information Criteria (BIC) was used to select the most parsimonious model to represent the system penalizing the number of calibrated parameters (Gideon, 1978), as follows:

$$BIC = nLN\left(\frac{SSE}{n}\right) + pLN(n) \quad (1)$$

where, LN is de natural log, n is the number of observations, p represents the number of calibrated parameters, and SSE is the sum of the residual error and the maximized likelihood function. Models with a lower BIC are preferred.

3.5. Storage and transit time estimates

Catchment storage is composed of a dynamic component hydraulically connected to the stream (Table 2 – the S reservoir variables calculated from the running water balance), and an additional passive mixing volume that is available for tracer mixing but does not contribute to streamflow. The dynamic storage component represents the water in each model reservoir above a certain threshold at which the reservoir starts contributing to the stream. The passive storage volume is a calibrated parameter for each reservoir that is only available for mixing tracers (stable isotopes) (Birkel et al., 2011; Staudinger et al., 2017). The sum of the dynamic and passive storage volume (total storage) was used to calculate transit times (TT, Eq. (2) based on the assumption that the catchment is a single unit that includes all the possible water flow pathways (Lazo et al., 2019; McMillan et al., 2012). Thus, the TT can be calculated as a lumped but time-variable catchment descriptor based on the catchment water balance (Lazo et al., 2019), using the discharge as the output for stationary processes (Eq. (2).), and discharge plus ET_a as the outputs for non-stationary processes (Eq. (3).).

$$TT = Storage/Q \quad (2)$$

$$TT = Storage/(Q + ET_a) \quad (3)$$

4. Results

4.1. Tracer-based multi-model simulation of páramo catchment dynamics

The six model conceptualizations of catchment hydrological behavior (Fig. 3, Table 2) yielded acceptable simulation of streamflow dynamics, with peak flows being well-represented (Fig. 4 – only Q). Nevertheless, the models that did not include an additional shallow fractured rock reservoir (models M1, M3, and M5) did not adequately reproduce hydrograph recessions and baseflow dynamics (Fig. 4: M1, M3, M5). In addition, models M5 and M6 that included slow and fast flow components on the hillslopes simulated the overall streamflow dynamics better than the simpler model configurations (models M1, M2, M3 and M4) (KGE ~ 0.9) (boxplot panel in Fig. 4).

Further testing of the models for isotope and DOC simulations (Fig. 5) showed that the simpler models 1–4 failed to adequately capture the tracer dynamics. Only model M6 resulted in a good streamflow-isotope simulations, while models M5 and M6 adequately simulated DOC. Most notably, the peak concentrations of both tracers were well represented by these models. Direct comparison of simulated and observed tracer dynamics (Fig. 5) showed that model M6 yielded the most accurate representation of stable isotopes and DOC in streamflow. These results confirmed the need to represent the páramo hydrological system by the dominant soil types (Andosols on the hillslopes and Histosols at valley bottoms) and with a shallow fractured bedrock reservoir that constantly contributes to total streamflow. The latter was even more evident during low flow periods (e.g., 11/2017 to 01/2018 and 10/2018 to 11/2018) and allowed an accurate simulation of the dynamics of discharge, conservative, and reactive tracers (Figs. 4 and 5).

4.2. Comparing tracer-based calibration targets

Fig. 6 shows the comparison of model performance (i.e., goodness-of-fit) for the six evaluated model structures (M1–M6) through the visualization of two-dimensional Pareto fronts (Fig. 6 a, b, c) and the distribution of model performance (Fig. 5 d, e, f) for the retained parameter sets after calibration using the three different calibration targets (i.e.,

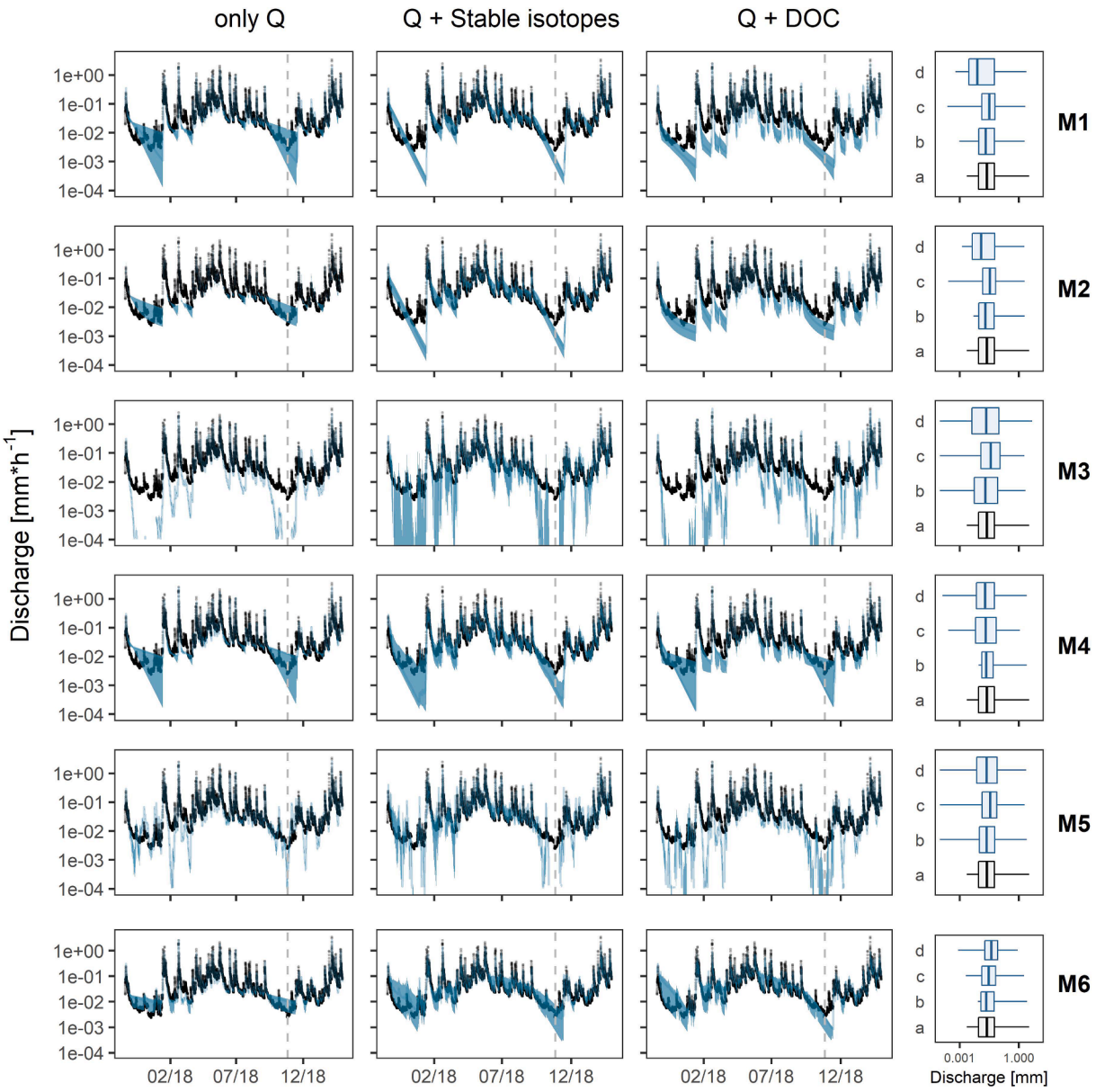

Fig. 4. Time series of observed (black) and predicted 5/95% uncertainty bounds (blue) of discharge. Each column represents the three different calibration targets used in the study. The first column represents calibration for discharge alone, the second column shows the simultaneous calibration of discharge and stable isotopes, and the third column displays the simultaneous calibration of discharge and DOC, for the six models presented in Fig. 3 and Table 2, with the simplest model in the upper row (M1) to the most complex model in the lowest row (M6). The last column shows a comparison of observed and simulated discharge using the three targets (a = observed discharge; b = only discharge; c = discharge + stable isotopes; c = discharge + DOC). The vertical dotted line in all plots separates calibration (October 2017–October 2018) and validation (November 2018–February 2019) periods. (For interpretation of the references to colour in this figure legend, the reader is referred to the web version of this article.)

with and without tracers). The Pareto fronts show that the most complex model (M6) outperformed the other five models for the only Q and the Q + stable isotopes calibration targets. For the Q + DOC calibration target, models 5 and 6 presented a similar discharge performance and outperformed the simpler models 1–4, but model 5 had a slightly better performance for DOC (KGE improvement ~ 0.05). This also had implications for the best parameter sets of the models (1 to 6), where the parameter sets for comparing the three calibration targets, were more consistent for the complex models (see Appendix).

When penalizing the models for the number of calibrated parameters to account for potential overparameterization, the BIC values in terms of discharge simulation (Fig. 7a) for the validation period were quite similar, with better results for models M6 (9 parameters; BIC = −17641) and M5 (6 parameters; BIC = −17630). When introducing stable isotopes as tracer in the models, models M2 (9 parameters; BIC = −17226) and M6 (13 parameters; BIC = −17059) led to the best results for discharge. When introducing DOC as tracer for model calibration, models M5 (13 parameters; BIC = −17043) and M4 (14 parameters; BIC = −16863) led to the best results.

For tracer simulations, model M6 (13 parameters for Q + Stable isotopes; BIC = 791) was the best model (Fig. 7a), despite the highest number of parameters compared to the other models. For the DOC simulations, models M5 (15 parameters; BIC = 514) and M6 (19 parameters; BIC = 1421) were the most parsimonious of all assessed models.

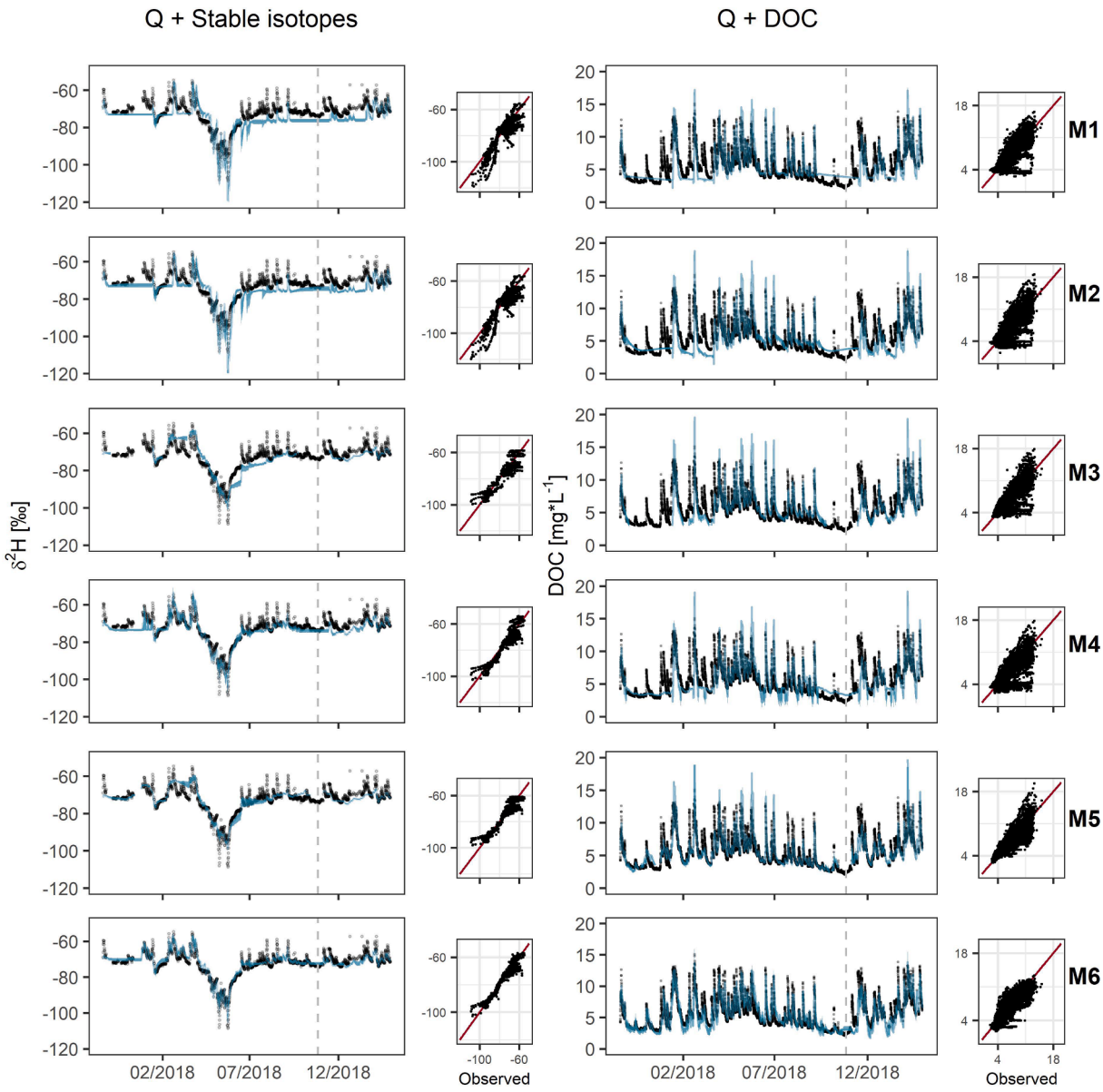

Fig. 5. Time series and scatter plots (showing the 1:1 line in red) of observed (black) vs. predicted 5/95% uncertainty bounds (blue) of tracers. The first two columns show the tracer simulation results when simultaneously calibrating the model on discharge and stable isotopes, whereas the third and fourth columns display the tracer simulation results when calibrating the model on discharge and DOC simultaneously for the six models presented in Fig. 3 and Table 2, from the simplest model (M1) in the upper row to the most complex model in the lowest row (M6). Vertical dotted line separates calibration and validation periods. (For interpretation of the references to colour in this figure legend, the reader is referred to the web version of this article.)

4.3. Water age, storage, fluxes and independent model evaluation

We compared the dynamic storage that hydraulically contributes to streamflow using the median of the best retained parameter sets for each model and calibration target (Table 3). Roughly, the dynamic storage varied from 10 mm to 106 mm for all models and targets and was almost an order of magnitude smaller than the passive storage (450 mm to 1220 mm). Thus the dynamic storage represented between 1% and 13% of the total storage. The highest dynamic storage of around 100 mm resulted from models M1 and M2 for all targets, whereas the dynamic storages from models M3 to M6 were smaller than 50 mm. Model M6 had the most consistent dynamic storage with less than 10 mm difference between the three calibration targets.

The passive storage and mean transit times of the best results of all models were significantly different (Wilcoxon Test; p value < 0.005) (Table 3). The largest passive storage (971–1216 mm) and resulting MTTs (649–813 days for stationary conditions, and 316–396 days for non-stationary conditions) values were obtained for model M4. Smaller passive storage (455–1014 mm) and MTTs (287–640 days for stationary conditions, and 144–321 days for non-stationary conditions) values coincided for model M2. Overall, MTTs were in the order of 9 months to 2.5 years for stationary conditions, and in the order of 5 months to 13 months for non-stationary conditions.

The separation of the simulated hydrograph into the sources contributing water to streamflow revealed the important contribution of deeper soil layers and shallow fractured rock during baseflow conditions (only Q = 18 %, Q + stable isotopes = 21 %, Q + DOC = 36 %) (Fig. 8). These water sources help to maintain streamflow during rain-free periods (Fig. 8, models 1, 2, 4, 6). This is most evident in models M3 and M5, which did not include a deep soil layer or shallow fractured rock water source and resulted in a poor representation of baseflow. However, wetter periods are consistently well simulated by all models for all

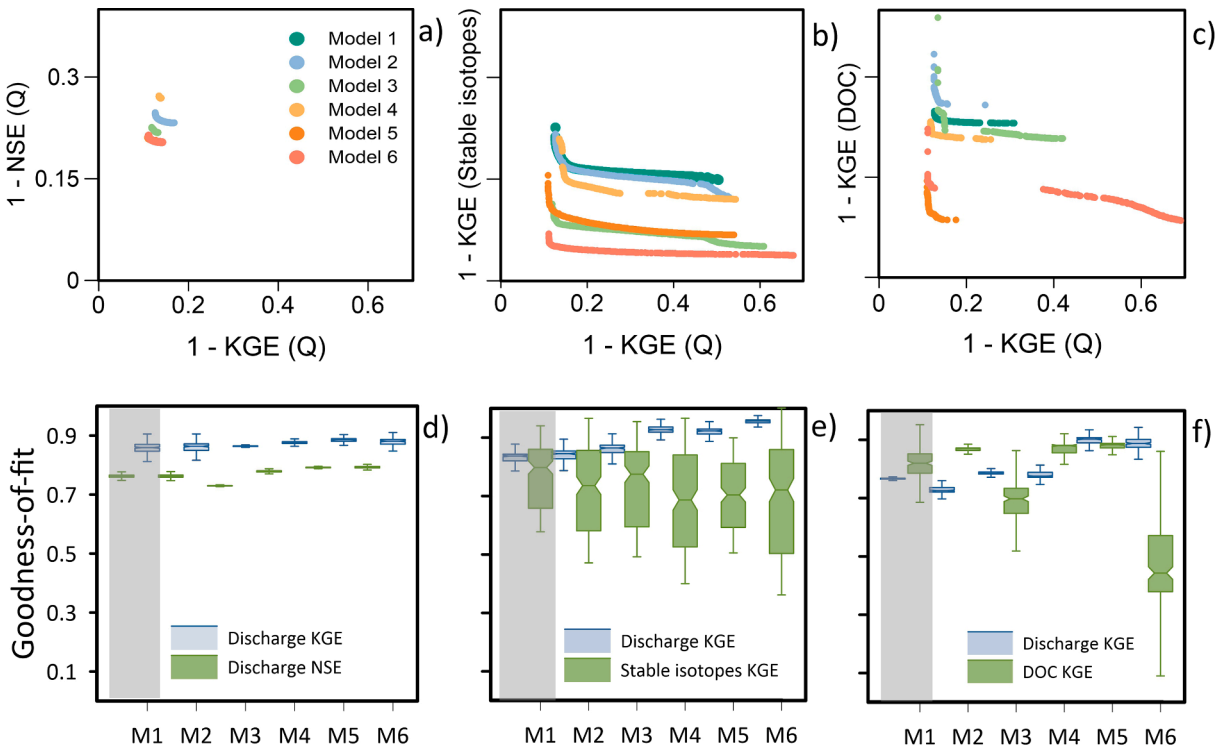

Fig. 6. Pareto diagrams (first row) and performance (i.e., goodness-of-fit; second row; KGE = Kling-Gupta efficiency, NSE = Nash-Sutcliffe efficiency) of the six models (from the simplest model (M1) to the more complex model (M6)) used to minimize the three calibration targets used in this study, i.e., discharge (Q) calibration alone (left), simultaneous calibration of Q and stable isotopes (center; D = deuterium or hydrogen-2), and simultaneous calibration of Q and dissolved organic carbon (DOC) (right). Gray bands highlight the simplest model as a reference.

calibration targets with water mainly originating from shallower and well-connected water sources.

We independently evaluated all proposed models by comparing their simulated dynamic storage with the temporal dynamics of observed soil water content (SWC). We rescaled the SWC values measured in the shallow Andosol horizon (Fig. 9), from the actual range (0–1 cm^3*cm^{-3}) to the storage range of the models (-50 to 100 mm), for comparison purposes the dynamic storage of all models was high and significant correlated with soil water content. The best linear regressions were found for the only discharge calibration target of model M2 ($R^2 = 0.88$; intercept = −2.5) followed by model M6 ($R^2 = 0.88$; intercept = −25). For the Q + stable isotopes calibration targets the best correlations were found for model M6 ($R^2 = 0.9$; intercept = −8) and models M5 and M2 ($R^2 = 0.84$; intercept = −3.06, and $R^2 = 0.84$; intercept = 5.02, respectively). For the Q + DOC target the best correlations were found for model M5 ($R^2 = 0.85$; intercept = 11) and models M2 and M4 ($R^2 = 0.85$; intercept = 13, and $R^2 = 0.85$; intercept = 17.4, respectively).

5. Discussion

5.1. Best model representation of the páramo hydrological system

Different rainfall-runoff model structures (i.e., multi-model framework) resulted in a very similar overall discharge model performance (Figs. 4 and 7); the very simple, 4-parameter model (e.g., model M1) was able to simulate streamflow almost equally well as the much more complex model (M6) with 9 parameters. However, there can be severe limitations of rainfall-runoff models in representing the water flow paths or catchment functioning even when discharge simulations are acceptable (Birkel and Soulsby, 2015; McGuire and McDonnell, 2015). If additional hydrological characteristics such as catchment storage, transit time, and hydrograph separation were considered, the advantages of tracer-aided hydrological models over only rainfall-runoff models become clear (cf. Christian Birkel and Soulsby, 2015; McGuire and McDonnell, 2015).

The independent model evaluation comparing dynamic storage and observed SWC showed qualitatively similar dynamics (Fig. 8), but the simulated storage was better represented with the most complex model (model M6) for all calibration targets (R - squared ≈ 0.93). The model performance comparisons (NSE and KGE) showed that the more complex models had an advantage over simpler ones, particularly when using tracers for model calibration (Fig. 6 and Fig. 9). Significant differences were observed among almost all groups of optimized KGE values (Kruskal-Wallis rank sum test; p-value < 0.001); however, the greatest differences were found for the tracer-aided model simulations (Fig. 6).

The tracer scatter plots (Fig. 5) clearly indicated the improvement of the simulations as the more complex models approach the 1:1 line. Thus, the more complex models (models M4, M5, M6) – that included flow through deep soil layers and shallow fractured rock, in addition to quicker near-surface runoff generation, outperformed other models. These findings support previous findings in this ecosystem that found that Andosols on hillslopes drain water to the valley bottom Histosols, which in turn contribute the bulk of water to discharge (Correa et al., 2019; Mosquera et al., 2016a). In addition, a shallow rock model reservoir was necessary to maintain baseflows during rain-free periods, similar to the results for nearby páramo catchments studied by Ramónet al. (2021) and Buytaert and Beven, (2011). Indeed, the thin layer of fractured rock observed in geological studies (ITASCA DENVER Inc., 2020), could play an important role in the hydrology of the páramo, similar to the rock moisture hypothesis by Rempe and Dietrich (2018). The latter was observed in a different geological setting with a more seasonal climate in California, USA and can be thought of as a more widespread global hydrological feature.

The fractured rock layer in our models generated 18–37 % of streamflow and was particularly important for baseflows. The

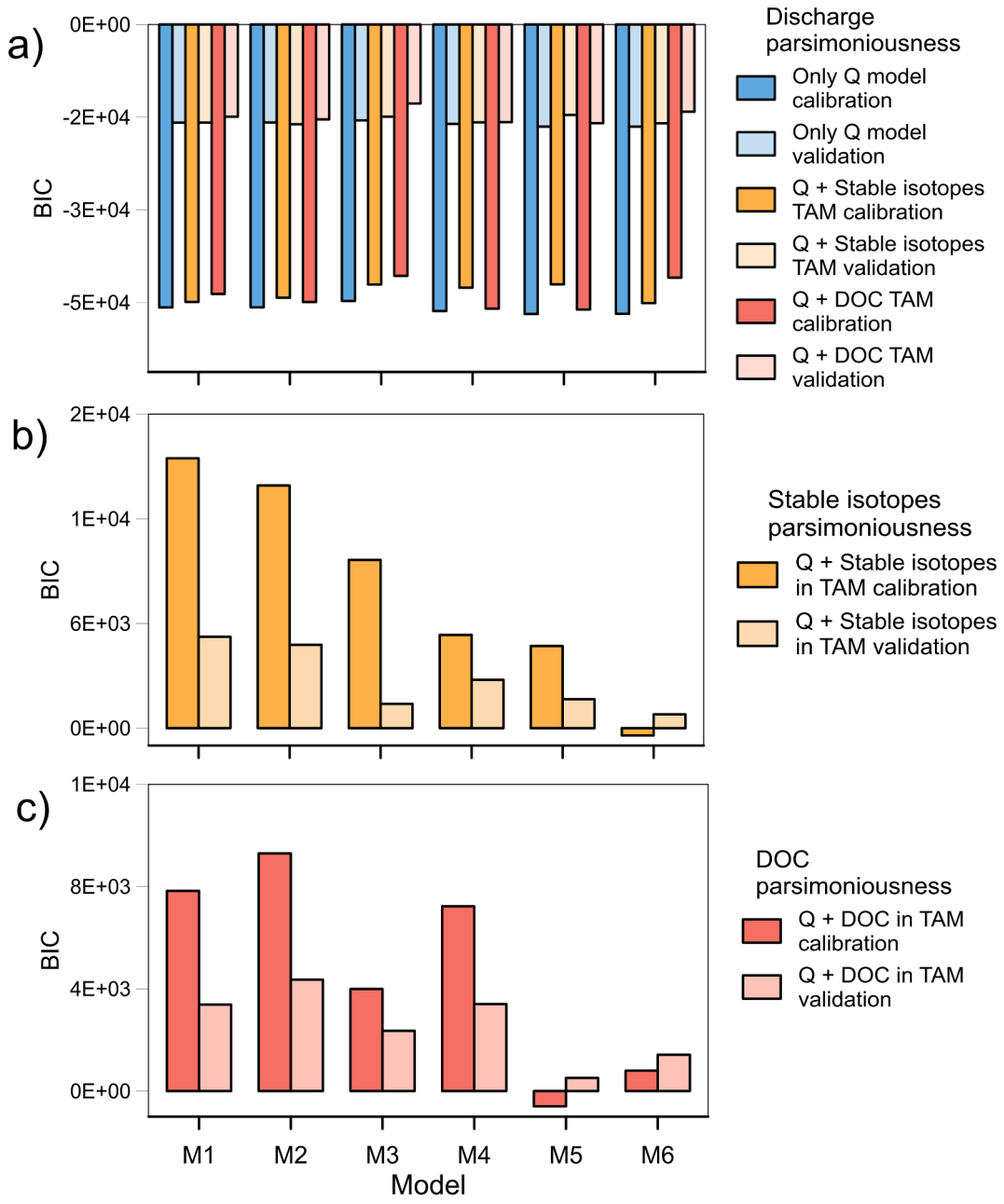

Fig. 7. Bar diagram of the Bayesian Information Criterion (BIC) results for a) discharge (Q) using the three calibration targets – i.e., Q calibration alone, simultaneous calibration of Q and stable isotopes, and simultaneous calibration of Q and dissolved organic carbon (DOC) – for the calibration and validations periods, b) stable isotopes during calibration and validations periods, and DOC for the calibration and validations periods. Results are presented for the six assessed models increasing in complexity and number of calibrated parameters (Table 2) from model M1 to model M6. TAM: tracer aided model.

contribution from this additional but disconnected reservoir can potentially contain waters > 1 year old (i.e., older than streamflow MTTs estimated at catchment scales, 6–9 months (Mosquera et al., 2016b) and causes non-stationary TTs, similar to other fast-responding systems in the tropics (Muñoz-Villers et al., 2016).

5.2. Biogeochemical dynamics in the páramo hydrological system

The hourly DOC data series included peaks or mobilization events, whose representation in most hydrological models remains a challenge (Blaurock et al., 2021; Ducharme et al., 2021; Werner et al., 2019), unless the dynamics of not only carbon production but also those of deposition and consumption in the hydrological system are adequately represented by the model (Aitkenhead et al., 2007; Rosset et al., 2020). In the páramo specifically, DOC production is more related to soil moisture conditions than to meteorological conditions (Pesántez et al., 2018), in contrast to other more temperate ecosystems (Birkel et al., 2017). The more complex models (models M5 and M6) that react only to the amount of water stored in each reservoir were successful at simulating DOC at high temporal resolution. The simpler models did not reproduce most of the quick production events in the Histosol reservoirs (Birkel et al., 2020; Pesántez et al., 2018; Wei et al., 2021), resulting in a lower model performance (Fig. 4). The latter supports evidence from previous observations in which wetting and rewetting events are directly related to high DOC concentrations in peat ecosystems (Fenner and Freeman, 2011; Tunaley et al., 2017). Lumped models or even the simple semi-distributed Histosol-Andosol models (models M1 - M4) could not accurately mimic DOC dynamics in the stream due to the fact

Table 3
Dynamic and passive storage and resulting mean transit time (MTT) based on equations 2–3 for the six evaluated models increasing in complexity from M1 to M6 (Table 2). For the dynamic storage the table shows the results for each calibration target. For passive storage and MTT we only show results from the discharge + stable isotopes calibration target.

	Calibration target	M1	M2	M3	M4	M5	M6
Dynamic Storage (mm)	**Discharge**	98 ± 7	97 ± 5	34 ± 1	51 ± 5	14 ± 1	29 ± 5
	Discharge + stable sotopes	103 ± 9	105 ± 11	17 ± 7	36 ± 6	11 ± 2	22 ± 4
	Discharge + DOC	81 ± 3	85 ± 3	26 ± 3	40 ± 4	15 ± 1	30 ± 6
Passive storage (mm)	**Discharge + stable isotopes (5/95 percentiles)**	658 ± 63	731 ± 183	639 ± 2	1170 ± 92	830 ± 85	992 ± 115
		510–714	455–1014	637–642	971–1216	719–963	855–1193
MTT (days)	**Discharge + stable isotopes (5/95 percentiles)**	417 ± 40	461 ± 116	428 ± 1	782 ± 61	528 ± 54	630 ± 73
Considering stationarity processes		323–452	287–640	427–430	649–813	458–613	542–757
MTT (days)	**Discharge + stable isotopes (5/95 percentiles)**	208 ± 18	231 ± 58	208 ± 1	381 ± 28	263 ± 27	314 ± 37
Considering non-stationarity processes		161–226	144–321	208–209	316–396	228–306	271–378

that the high production of carbon in the shallow soils needs to be accompanied by consumption-deposition processes in the deeper soils, which were not represented by the simplest models. The latter was also visible from the Pareto fronts in Fig. 6. Even model 6, that resulted in acceptable discharge and DOC simulations showed a trade-off effects with slightly lower discharge performance at the expense of satisfying two calibration targets (Fowler et al., 2018). In addition, we believe that including dispersion and partial mixing processes into simple conceptual models can give additional insights into the functioning of catchment systems (Fenicia et al., 2010; Hrachowitz et al., 2013), but crucially depends on future data availability for different soil water pools to help with model parameterization.

DOC export rate estimates yielded by the six models were similar to those measured previously in the study catchment (48.4 Kg ha^{-1} yr^{-1}) (Arízaga-Idrovo et al., 2022). From all the models, export rates obtained from model M6 calibrated on the discharge and DOC targets represented the observations best (model M1: 62.6 Kg ha^{-1} yr^{-1}; model M2: 61.6 Kg ha^{-1} yr^{-1}; model M3: 64.6 Kg ha^{-1} yr^{-1}; model M4: 59.1 Kg ha^{-1} yr^{-1}; model M5: 58.5 Kg ha^{-1} yr^{-1}; model M6: 45.4 Kg ha^{-1} yr^{-1}).

The representation of lateral flow, rewetting processes, and riparian areas as DOC production hotspots, strongly influenced the carbon export from the catchment, highlighting possible consequences of climate and land use change on water quantity/quality of the páramo ecosystem (Pesántez et al., 2018). Such results could only have been produced by direct comparison of different model structures and a temporally high-resolution data set (Fig. 4 and Fig. 8). In this sense, our proposed, more complex models resolved limitations of previous studies in approximating flow and tracer dynamics particularly at low flows in the páramo (Cabrera-balarezo et al., 2022; Gil and Tobón, 2016; Vázquez, 2010).

5.3. Multi-model catchment storage and TT simulations

Modelled dynamic storage, was similar to that estimated from hydrological data in the study catchment (Lazo et al., 2019), particularly for model M6. Important differences emerged when comparing the results derived for total storage (including passive storage mixing volumes) for model M6 (855–1193 mm) and those calculated from streamflow mean transit time estimates (445 mm) in the same catchment based on the catchment water balance (Lazo et al., 2019). Our results can be compared to Lazoet al. (2019) specifically to their calculated soil horizon passive storages (854 mm). A possible explanation for storage differences is that some flow paths are not hydrologically active when calculating TTs and storage (Birkel et al., 2011; Kirchner, 2009). However, our results are comparable to others for peat dominated catchments (Amvrosiadi et al., 2017; van Huijgevoort et al., 2016). The latter studies accounted for all the water available for mixing and not only the shallow hydrologically active flow paths (cf. McGuire and McDonnell, 2015; Soulsby et al., 2009). It seems that in comparison to tracer aided hydrological model estimates, calculations based on soil properties of the hydrologically active layers, lead to an underestimation of total storage (Bishop et al., 2011; Guangxuan et al., 2021). Furthermore, different methods to estimate storage can yield different transit times (Staudinger et al., 2017). Most common rainfall-runoff models only consider the hydraulically active soil and groundwater contributions to streamflow.

Related to the higher storage estimates, our calculated transit times calculated assuming stationary conditions (542 to 757 days) using the most parsimonious model (model M6) were longer than those previously reported for the same catchment using lumped convolution integral models (~188 days) (Lazo et al., 2019; Mosquera et al., 2016b). This difference is likely related to the fact that the tracer-aided hydrological models consider the system as a whole, including potential non-stationary changes in water storage associated to flow paths under different catchment wetness conditions (Cain et al., 2019; Heidbüchel et al., 2012; Staudinger et al., 2017). Transit times calculated under non-stationary conditions already found in this catchment by Larcoet al. (2023), were much closer to those found previously using lumped convolution integral models (Larco et al., 2023; Mosquera et al., 2016b). In addition, we identified an additional reservoir (shallow fractured rock) which generates a significant volume of water (18–37 %) to the stream during baseflow conditions, increasing transit times and related passive storage.

Our results improve the understanding of páramo catchment hydrology and biogeochemistry, while highlighting the benefit of including tracers into conceptual rainfall-runoff models to enhance hydrobiogeochemical process knowledge (Kirchner, 2006). The results indicate that due to the compact geology, and low precipitation volumes distributed throughout the year small changes in climate or land use directly affect the soil water dynamics, with likely significant affect the páramo ecohydrology (e.g., export of carbon and other associated solutes). Therefore, future work should focus on a spatial analysis of DOC generation hotspots in the catchment assessing DOC source contributions to streamflow carbon export.

6. Conclusions and outlook

This study presents for the first time a complete suite of rainfall-runoff models of different complexity to conceptualize the hydrological behavior of an experimental páramo catchment in the tropical Andean highlands of southern Ecuador. The incorporation of conservative (stable isotopes) and reactive (DOC) tracers into these models helped to assess the hydrological and biogeochemical catchment functioning of the páramo. Models of higher complexity outperformed the simpler

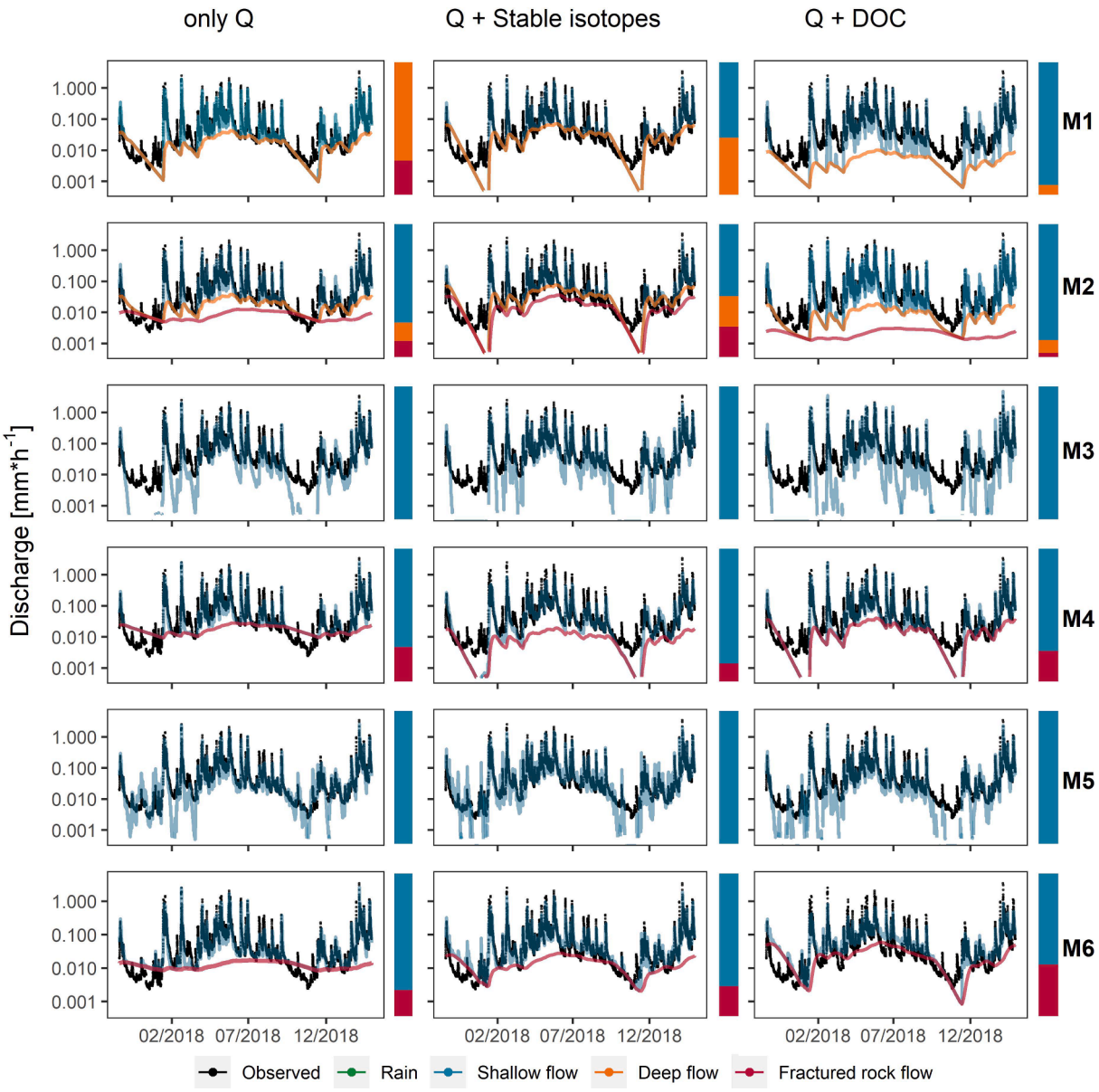

Fig. 8. Time series of the simulated water source fluxes for the best fitting parameter sets. Each column represents one of the three different calibration targets used in the study. The first column represents calibration for discharge alone, the second column shows the simultaneous calibration of discharge and stable isotopes, and the third column displays the simultaneous calibration of discharge and DOC for the six models presented in Fig. 3 and Table 2, from the simplest model (M1) in the upper row to the most complex model in the lowest row (M6). Observed discharge is shown in black, while the other colored lines correspond to the fluxes that directly contribute to discharge. The bar charts display the fraction (0, 1) contributed by each source to streamflow. Lines for the sources are cumulative from the lowest to the highest value. The vertical dotted line in all plots separates calibration (October 2017–October 2018) and validation (November 2018–February 2019) periods.

ones, when introducing tracers for calibration. Our simulations identified the importance of flow through deep soil layers and shallow fractured rock to sustain streamflow generation during drier periods (baseflow). This finding was only possible by including a (conservative) tracer module in the rainfall-runoff model structures. Tracer-based simulations clearly showed a mix of fast and slow flows generated from the shallow and deeper soil layers of Histosols and Andosols, in combination with water from a shallow fractured rock layer on top of the compact bedrock. These results were consistent for both tracer calibration targets (discharge + stable isotopes and discharge + DOC) but for slightly different reasons. The biogeochemical module simulated DOC dynamics at high temporal resolution based only on the modeled soil water content without the need of including temperature as a predictor for DOC production, but the estimated DOC mass flux depends on the accurate simulation of the combination of flow paths as identified with stable isotopes. Based on our findings, we conclude that tracer selection depends on the specific objectives and study purpose as each have advantages and limitations in field experimental design and analytical cost. To bridge the gap from hydrological to biogeochemical catchment, functioning incorporation of both tracers into models is crucially needed.

CRediT authorship contribution statement

Juan Pesántez: Conceptualization, Methodology, Software, Validation, Formal analysis, Investigation, Data curation, Writing – original draft, Visualization. **Christian Birkel:** Validation, Methodology, Writing – review & editing, Supervision. **Giovanny M. Mosquera:**

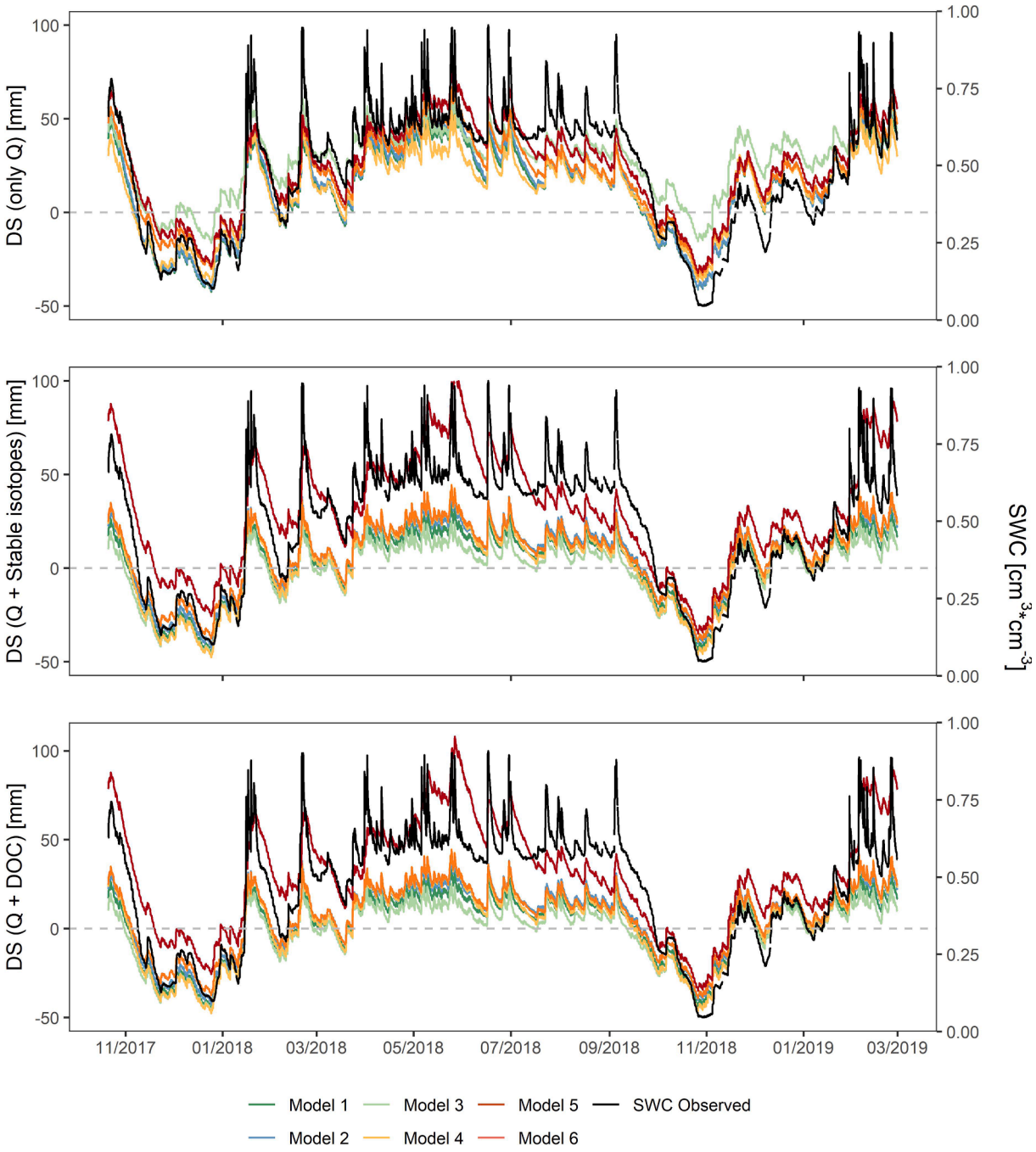

Fig. 9. Time series of dynamic storage corresponding to the best simulated discharge for the six models presented in Fig. 3 and Table 2 (from the simplest model M1 to the most complex model M6) and observed soil water content (SWC in black) during the study period (October 2017 - February 2019). Dynamic storage (DS) is plotted on the left Y-axis, and soil water content is plotted on the right Y-axis. The horizontal dotted line is the modeled threshold at which soil water contribution to streamflow starts.

Validation, Writing – review & editing. **Rolando Célleri:** Validation, Writing – review & editing, Supervision. **Pablo Contreras:** Software. **Irene Cárdenas:** Resources. **Patricio Crespo:** Conceptualization, Validation, Writing – review & editing, Supervision, Project administration, Funding acquisition.

Declaration of Competing Interest

The authors declare the following financial interests/personal relationships which may be considered as potential competing interests: Patricio Crespo reports financial support was provided by International Atomic Energy Agency (IAEA). Patricio Crespo reports financial support was provided by the Vice-Rectorate for Research of the University of Cuenca (Vicerrectorado de Investigación de la Universidad de Cuenca, VIUC). Patricio Crespo reports financial support was provided by the German Research Foundation (DFG).

Data availability

Data will be made available on request.

Acknowledgements

This manuscript is an outcome of the of the Doctoral Program in

Water Resources, offered by Universidad de Cuenca, Escuela Politécnica Nacional, and Universidad Técnica Particular de Loja. The research was founded by the projects "Evaluation of Non Stationary Hydrological Conditions in the Andean Páramo" founded by the IAEA (research contract 22906) and the Vice-Rectorate for Research of the University of Cuenca (Vicerrectorado de Investigación de la Universidad de Cuenca, VIUC), and "From field scale eco-hydrological process understanding to landscape scale water fluxes" founded by the DFG (Project number 386807763) and the VIUC. We thank Comuna Chumblín Sombrederas (San Fernando, Azuay) for the access to its communal land reserve. Many thanks to the researchers and staff of the Departamento de Recursos Hídricos y Ciencias Ambientales (iDRHiCA), which contributed to data collection. G.M.M. is supported by a Postdoctoral Fellowship from the Universidad San Francisco de Quito USFQ and the H2020 European Research and Innovation action Grant Agreement 869226 (DRYvER). We would also like to acknowledge the many suggestions and constructive comments by the Editor Sally Thompson and two anonymous reviewers that helped to shape the final version of this paper.

Appendix A. Supplementary data

Supplementary data to this article can be found online at https://doi.org/10.1016/j.jhydrol.2023.129328.

References

Aitkenhead, M.J., Aitkenhead-Peterson, J.A., McDowell, W.H., Smart, R.P., Cresser, M.S., 2007. Modelling DOC export from watersheds in Scotland using neural networks. Comput. Geosci. 33 (3), 423–436. https://doi.org/10.1016/j.cageo.2006.08.002.

Amvrosiadi, N., Seibert, J., Grabs, T., Bishop, K., 2017. Water storage dynamics in a till hillslope: the foundation for modeling flows and turnover times. Hydrol. Process. 31 (1), 4–14. https://doi.org/10.1002/hyp.11046.

Aparecido, L.M.T., Teodoro, G.S., Mosquera, G., Brum, M., de Barros, F.V., Pompeu, P.V., Rodas, M., Lazo, P., Müller, C.S., Mulligan, M., Asbjornsen, H., Moore, G.W., Oliveira, R.S., 2017. Ecohydrological drivers of Neotropical vegetation in montane ecosystems. Ecohydrology e1932. https://doi.org/10.1002/eco.1932.

Arízaga-Idrovo, V., Pesántez, J., Birkel, C., Peña, P., Mora, E., Crespo, P., 2022. Characterizing solute budgets of a tropical Andean páramo ecosystem. Sci. Environ. 835, 155560.

Beven, K.J., Chappell, N.A., 2021. Perceptual perplexity and parameter parsimony. Wiley Interdiscip. Rev. Water 8 (4), 1–19. https://doi.org/10.1002/wat2.1530.

Beven, K.J. 2012. Rainfall-runoff modelling: the primer. In *Rainfall-Runoff Modelling: The Primer: Second Edition*. 10.1002/9781119951001.

Birkel, C., Soulsby, C., Tetzlaff, D., 2011. Modelling catchment-scale water storage dynamics: Reconciling dynamic storage with tracer-inferred passive storage. Hydrol. Process. 25 (25), 3924–3936. https://doi.org/10.1002/hyp.8201.

Birkel, C., Soulsby, C., 2016. Linking tracers, water age and conceptual models to identify dominant runoff processes in a sparsely monitored humid tropical catchment. Hydrol. Process. 30 (24), 4477–4493. https://doi.org/10.1002/hyp.10941.

Birkel, C., Soulsby, C., Tetzlaff, D., 2014. Integrating parsimonious models of hydrological connectivity and soil biogeochemistry to simulate stream DOC dynamics. J. Geophys. Res.: Biogeosci. 119, 1861–1878. https://doi.org/10.1002/2014JG002705.Received.

Birkel, C., Broder, T., Biester, H., 2017. Nonlinear and threshold-dominated runoff generation controls DOC export in a small peat catchment. J. Geophys. Res. Biogeo. 122 (3), 498–513. https://doi.org/10.1002/2016JG003621.

Birkel, C., Duvert, C., Correa, A., Munksgaard, N.C., Maher, D.T., Hutley, L.B., 2020. Tracer-aided modeling in the low-relief, wet-dry tropics suggests water ages and DOC export are driven by seasonal wetlands and deep groundwater. Water Resour. Res. 56 (4) https://doi.org/10.1029/2019WR026175.

Birkel, C., Soulsby, C., 2015. Advancing tracer-aided rainfall-runoff modelling: A review of progress, problems and unrealised potential. Hydrol. Process. 29 (25), 5227–5240. https://doi.org/10.1002/hyp.10594.

Bishop, K., Seibert, J., Nyberg, L., Rodhe, A., 2011. Water storage in a till catchment. II: Implications of transmissivity feedback for flow paths and turnover times. Hydrol. Process. 25, 3950–3959. https://doi.org/10.1002/hyp.8355.

Blaurock, K., Beudert, B., Gilfedder, B., Fleckenstein, J., Peiffer, S., Hopp, L., 2021. Missing connectivity during summer drought controls DOC mobilization and export in a small, forested catchment. Hydrol. Earth Syst. Sci. Discuss. February, 1–30.

Bradley, R.S., Vuille, M., Diaz, H.F., Vergara, W., 2006. Threats to water supplies in the tropical Andes. Science 312 (5781), 1755–1756. https://doi.org/10.1126/science.1128087.

Buytaert, W., Beven, K., 2011. Models as multiple working hypotheses: Hydrological simulation of tropical alpine wetlands. Hydrol. Process. 25 (11), 1784–1799. https://doi.org/10.1002/hyp.7936.

Buytaert, W., Wyseure, G., De Bièvre, B., Deckers, J., 2005. The effect of land-use changes on the hydrological behaviour of Histic Andosols in south Ecuador. Hydrol. Process. 19, 3985–3997. https://doi.org/10.1002/hyp.5867.

Buytaert, W., Célleri, R., De Bièvre, B., Cisneros, F., Wyseure, G., Deckers, J., Hofstede, R., 2006a. Human impact on the hydrology of the Andean páramos. Earth Sci. Rev. 79 (1–2), 53–72. https://doi.org/10.1016/j.earscirev.2006.06.002.

Buytaert, W., Deckers, J., Wyseure, G., 2006b. Description and classification of nonallophanic Andosols in south Ecuadorian alpine grasslands (páramo). Geomorphology 73 (3–4), 207–221. https://doi.org/10.1016/j.geomorph.2005.06.012.

Cabrera-Balarezo, J.J., Sucozhañay-Calle, A.E., Crespo-Sánchez, P.J., Timbe-Castro, L.M., 2022. Applying hydrological modeling to unravel the effects of land use change on the runoff of a paramo ecosystem • Aplicación de modelamiento hidrológico para desentrañar los efectos del cambio de uso de la tierra en la escorrentía de un ecosistema de páramo. DYNA 89 (221), 68–77.

Cain, M.R., Ward, A.S., Hrachowitz, M., 2019. Ecohydrologic separation alters interpreted hydrologic stores and fluxes in a headwater mountain catchment. Hydrol. Process. 33 (20), 2658–2675. https://doi.org/10.1002/hyp.13518.

Carrillo-Rojas, G., Silva, B., Rollenbeck, R., Célleri, R., Bendix, J., 2019. The breathing of the Andean highlands: Net ecosystem exchange and evapotranspiration over the páramo of southern Ecuador. Agric. For. Meteorol. 265, 30–47. https://doi.org/10.1016/j.agrformet.2018.11.006.

Celleri, R., Feyen, J., 2009. The hydrology of tropical Andean ecosystems: importance, knowledge status, and perspectives. Mt. Res. Dev. 29 (4), 350–355. https://doi.org/10.1659/mrd.00007.

Chow, A.T., Tanji, K.K., Gao, S., 2003. Production of dissolved organic carbon (DOC) and trihalomethane (THM) precursor from peat soils. Water Res. 37 (18), 4475–4485. https://doi.org/10.1016/S0043-1354(03)00437-8.

Clark, M.P., Kavetski, D., Fenicia, F., 2011. Pursuing the method of multiple working hypotheses for hydrological modeling. Water Resour. Res. 47 (9), 1–16. https://doi.org/10.1029/2010WR009827.

Clark, M.P., Nijssen, B., Lundquist, J.D., Kavetski, D., Rupp, D.E., Woods, R.A., Freer, J.E., Gutmann, E.D., Wood, A.W., Brekke, L.D., Arnold, J.R., Gochis, D.J., Rasmussen, R.M., 2015. A unified approach for process-based hydrologic modeling: 1. Modeling concept. *Water Resour. Res.* 51 (4), 2498–2514.

Clark, M.P., Bierkens, M.F.P., Samaniego, L., Woods, R.A., Uijlenhoet, R., Bennett, K.E., Pauwels, V.R.N., Cai, X., Wood, A.W., Peters-Lidard, C.D., 2017. The evolution of process-based hydrologic models: Historical challenges and the collective quest for physical realism. Hydrol. Earth Syst. Sci. 21 (7), 3427–3440. https://doi.org/10.5194/hess-21-3427-2017.

Coltorti, M., Ollier, C.D., 2000. Geomorphic and tectonic evolution of the Ecuadorian Andes. Geomorphology 32 (1–2), 1–19. https://doi.org/10.1016/S0169-555X(99)00036-7.

Córdova, M., Célleri, R., Shellito, C.J., Orellana-Alvear, J., Abril, A., Carrillo-Rojas, G., 2016. Near-surface air temperature lapse rate over complex terrain in the Southern Ecuadorian Andes: Implications for temperature mapping. Arct. Antarct. Alp. Res. 48 (4), 678–684. https://doi.org/10.1657/AAAR0015-077.

Correa, A., Windhorst, D., Tetzlaff, D., Patricio, C., Celleri, R., Feyen, J., Breuer, L., 2017. Temporal dynamics in dominant runoff sources and flow paths in the Andean Páramo. Water Resour. Res. 53, 5998–6017. https://doi.org/10.1002/2016WR020187.

Correa, A., Breuer, L., Crespo, P., Célleri, R., Feyen, J., Birkel, C., Silva, C., Windhorst, D., 2019. Spatially distributed hydro-chemical data with temporally high-resolution is needed to adequately assess the hydrological functioning of headwater catchments. Sci. Total Environ. 651, 1613–1626. https://doi.org/10.1016/j.scitotenv.2018.09.189.

Correa, A., Ochoa-Tocachi, B.F., Birkel, C., Ochoa-Sánchez, A., Zogheib, C., Tovar, C., Buytaert, W., 2020. A concerted research effort to advance the hydrological understanding of tropical páramos. Hydrol. Process. 34 (24), 4609–4627. https://doi.org/10.1002/hyp.13904.

Crespo, P., Feyen, J., Buytaert, W., Celleri, R., Frede, H.G., Ramirez, M., Breuer, L., 2012. Development of a conceptual model of the hydrologic response of tropical Andean micro-catchments in Southern Ecuador. HESS 2475–2510. https://doi.org/10.5194/hessd-9-2475-2012.

Dams, J., Nossent, J., Senbeta, T.B., Willems, P., Batelaan, O., 2015. Multi-model approach to assess the impact of climate change on runoff. J. Hydrol. 529, 1601–1616. https://doi.org/10.1016/j.jhydrol.2015.08.023.

Deb, K., Pratap, A., Agarwal, S., Meyarivan, T., 2002. A fast and elitist multiobjective genetic algorithm: NSGA-II. IEEE Trans. Evol. Comput. 6 (2), 182–197. https://doi.org/10.1109/4235.996017.

DeForest, D.K., Brix, K.V., Tear, L.M., Adams, W.J., 2018. Multiple linear regression models for predicting chronic aluminum toxicity to freshwater aquatic organisms and developing water quality guidelines. Environ. Toxicol. Chem. 37 (1), 80–90. https://doi.org/10.1002/etc.3922.

Dick, J.J., Tetzlaff, D., Birkel, C., Soulsby, C., 2015. Modelling landscape controls on dissolved organic carbon sources and fluxes to streams. Biogeochemistry 122 (2–3), 361–374. https://doi.org/10.1007/s10533-014-0046-3.

Ducharme, A.A., Casson, N.J., Higgins, S.N., Friesen-Hughes, K., 2021. Hydrological and catchment controls on event-scale dissolved organic carbon dynamics in boreal headwater streams. Hydrol. Process. 35 (7).

Esquivel-Hernández, G., Sánchez-Murillo, R., Quesada-Román, A., Mosquera, G., Birkel, C., Boll, J., 2018. Insight into the stable isotopic composition of glacial lakes in a tropical alpine ecosystem: Chirripó, Costa Rica. Hydrol. Process. 32 (24), 3588–3603. https://doi.org/10.1002/hyp.13286.

Fenicia, F., Wrede, S., Kavetski, D., Pfister, L., Hoffmann, L., Savenije, H.H.G., McDonnell, J.J., 2010. Assessing the impact of mixing assumptions on the estimation

of streamwater mean residence time. Hydrol. Process. 24 (12), 1730–1741. https://doi.org/10.1002/hyp.7595.
Fenner, N., Freeman, C., 2011. Drought-induced carbon loss in peatlands. Nat. Geosci. 4 (12), 895–900. https://doi.org/10.1038/ngeo1323.
Fowler, K., Coxon, G., Freer, J., Peel, M., Wagener, T., Western, A., Woods, R., Zhang, L., 2018. Simulating runoff under changing climatic conditions: A framework for model improvement. Water Resour. Res. 54 (12), 9812–9832. https://doi.org/10.1029/2018WR023989.
Freeman, C., Evans, C.D., Monteith, D.T. 2001. Export of organic carbon from peat soils. *Nature*, *412*, 785–786. 10.1038/35090628.
Gideon, S., 1978. Estimating the dimension of a model. Ann. Stat. 6 (2), 461–464.
Gil, E.G., Tobón, C., 2016. Hydrological modelling with TOPMODEL of chingaza páramo, Colombia. Revista Facultad Nacional de Agronomia Medellin 69 (2), 7919–7933. https://doi.org/10.15446/rfna.v69n2.59137.
Guallpa, M., Rolando, C., Crespo, P., 2022. Efecto del coeficiente teórico de descarga de vertederos sobre la medición de caudales en pequeños ríos Andinos. La Granja 36 (2).
Guangxuan, L., Xi, C., Zhicai, Z., Lichun, W., Chris, S. 2021. Effects of passive storage on modelling hydrological function and isotope dynamics in a karst flow system in southwest China. *Hydrol. Earth Syst. Sci.*, *December*, 1–47.
Gupta, H.V., Kling, H., Yilmaz, K.K., Martinez, G.F., 2009. Decomposition of the mean squared error and NSE performance criteria: Implications for improving hydrological modelling. J. Hydrol. 377 (1–2), 80–91. https://doi.org/10.1016/j.jhydrol.2009.08.003.
Gutiérrez-Salazar, P., Medrano-Vizcaíno, P., 2019. The effects of climate change on decomposition processes in Andean Paramo ecosystem-synthesis, a systematic review. Appl. Ecol. Environ. Res. 17 (2), 4957–4970. https://doi.org/10.15666/aeer/1702_49574970.
Heidbüchel, I., Troch, P.A., Lyon, S.W., Weiler, M., 2012. The master transit time distribution of variable flow systems. Water Resour. Res. 48 (6) https://doi.org/10.1029/2011WR011293.
Hrachowitz, M., Savenije, H., Bogaard, T.A., Tetzlaff, D., Soulsby, C., 2013. What can flux tracking teach us about water age distribution patterns and their temporal dynamics? Hydrol. Earth Syst. Sci. 17 (2), 533–564. https://doi.org/10.5194/hess-17-533-2013.
Hrachowitz, M., Benettin, P., van Breukelen, B.M., Fovet, O., Howden, N.J.K., Ruiz, L., van der Velde, Y., Wade, A.J., 2016. Transit times—the link between hydrology and water quality at the catchment scale. Wiley Interdiscip. Rev. Water 3 (5), 629–657. https://doi.org/10.1002/wat2.1155.
ITASCA DENVER Inc. (2020). *Loma Larga Groundwater and Geochemistry EIA Support.*
Kirchner, J.W., 2006. Getting the right answers for the right reasons: Linking measurements, analyses, and models to advance the science of hydrology. Water Resour. Res. 42 (3), 1–5. https://doi.org/10.1029/2005WR004362.
Kirchner, J.W., 2009. Catchments as simple dynamical systems: Catchment characterization, rainfall-runoff modeling, and doing hydrology backward. Water Resour. Res. 45 (2), 1–34. https://doi.org/10.1029/2008WR006912.
Larco, K., Mosquera, G.M., Jacobs, S.R., Cardenas, I., Crespo, P., 2023. Factors controlling the temporal variability of streamflow transit times in tropical alpine catchments. J. Hydrol. 617 (PB), 128990 https://doi.org/10.1016/j.jhydrol.2022.128990.
Lazo, P.X., Mosquera, G.M., McDonnell, J.J., Crespo, P., 2019. The role of vegetation, soils, and precipitation on water storage and hydrological services in Andean Páramo catchments. J. Hydrol. 572, 805–819. https://doi.org/10.1016/j.jhydrol.2019.03.050.
Mcdonnell, J.J., Beven, K., 2014. Debates—The future of hydrological sciences: A (common) path forward? A call to action aimed at understanding velocities, celerities and residence time distributions of the headwater hydrograph. Water Resour. Res. 50 (6), 5342–5350. https://doi.org/10.1002/2013WR015141.
Mcdonnell, J.J., Bonell, M., Stewart, M.K., Pearce, A.J., 1990. Implications for stream hydrograph separation. Water Resour. Res. 26 (3), 455–458.
McGuire, K.J., McDonnell, J.J., 2015. Tracer advances in catchment hydrology. Hydrol. Process. 29 (25), 5135–5138. https://doi.org/10.1002/hyp.10740.
McMillan, H., Tetzlaff, D., Clark, M., Soulsby, C., 2012. Do time-variable tracers aid the evaluation of hydrological model structure? A multimodel approach. Water Resour. Res. 48 (5) https://doi.org/10.1029/2011WR011688.
Messerli, B., Viviroli, D., Weingartner, R., 2004. Mountains of the world: Vulnerable water towers for the 21st century. Ambio 33 (SPEC. ISS. 13), 29–34. https://doi.org/10.1007/0044-7447-33.sp13.29.
Mora, D.E., Campozano, L., Cisneros, F., Wyseure, G., Willems, P., 2014. Climate changes of hydrometeorological and hydrological extremes in the Paute basin, Ecuadorean Andes. Hydrol. Earth Syst. Sci. 18 (2), 631–648. https://doi.org/10.5194/hess-18-631-2014.
Mosquera, G.M., Lazo, P.X., Célleri, R., Wilcox, B.P., Crespo, P., 2015. Runoff from tropical alpine grasslands increases with areal extent of wetlands. Catena 125, 120–128. https://doi.org/10.1016/j.catena.2014.10.010.
Mosquera, G.M., Célleri, R., Lazo, P.X., Vaché, K.B., Perakis, S.S., Crespo, P., 2016a. Combined use of isotopic and hydrometric data to conceptualize ecohydrological processes in a high-elevation tropical ecosystem. Hydrol. Process. 30 (17), 2930–2947. https://doi.org/10.1002/hyp.10927.
Mosquera, G.M., Segura, C., Vaché, K., Windhorst, D., Breuer, L., Crespo, P., 2016b. Insights into the water mean transit time in a high-elevation tropical ecosystem. Hydrol. Earth Syst. Sci. 20 (7), 2987–3004. https://doi.org/10.5194/hess-20-2987-2016.
Mosquera, G.M., Franklin, M., Jan, F., Rolando, C., Lutz, B., David, W., Patricio, C., 2021. A field, laboratory, and literature review evaluation of the water retention curve of volcanic ash soils: How well do standard laboratory methods reflect field conditions? Hydrol. Process. 35 (1) https://doi.org/10.1002/hyp.14011.
Muñoz-Villers, L.E., Geissert, D.R., Holwerda, F., McDonnell, J.J., 2016. Factors influencing stream baseflow transit times in tropical montane watersheds. Hydrol. Earth Syst. Sci. 20 (4), 1621–1635. https://doi.org/10.5194/hess-20-1621-2016.
Ochoa-Sánchez, A., Crespo, P., Célleri, R., 2018. Quantification of rainfall interception in the high Andean tussock grasslands. Ecohydrology 11 (3). https://doi.org/10.1002/eco.1946.
Ochoa-Tocachi, B., Buytaert, W., De Bièvre, B., Célleri, R., Crespo, P., Villacís, M., Llerena, C., Acosta, L., Villazón, M., Guallpa, M., Gil-Ríos, J., Fuentes, P., Olaya, D., Viñas, P., Rojas, G., Arias, S., 2016. Impacts of land use on the hydrological response of tropical Andean catchments. Hydrol. Process. 30 (22), 4074–4089.
Ouyang, Y., Nkedi-Kizza, P., Wu, Q.T., Shinde, D., Huang, C.H., 2006. Assessment of seasonal variations in surface water quality. Water Res. 40 (20), 3800–3810. https://doi.org/10.1016/j.watres.2006.08.030.
Padrón, R.S., Wilcox, B.P., Crespo, P., Célleri, R., 2015. Rainfall in the Andean Páramo: New insights from high-resolution monitoring in southern Ecuador. J. Hydrometeorol. 16 (3), 985–996. https://doi.org/10.1175/JHM-D-14-0135.1.
Patiño, S., Hernández, Y., Plata, C., Domínguez, I., Daza, M., Oviedo-Ocaña, R., Buytaert, W., Ochoa-Tocachi, B.F., 2021. Influence of land use on hydro-physical soil properties of Andean páramos and its effect on streamflow buffering. Catena 202, 105227. https://doi.org/10.1016/j.catena.2021.105227.
Pesántez, J., Mosquera, G.M., Crespo, P., Breuer, L., Windhorst, D., 2018. Effect of land cover and hydro - meteorological controls on soil water DOC concentrations in a high - elevation tropical environment. Hydrol. Process. 32 (17), 2624–2635. https://doi.org/10.1002/hyp.13224.
Pesántez, J., Birkel, C., Mosquera, G.M., Peña, P., Arizaga, V., Mora, E., McDowell, W.H., Crespo, P., 2021. High-frequency multi-solute calibration using an in situ UV-visible sensor. Hydrol. Process., e14357 https://doi.org/10.1002/HYP.14357.
Pfister, L., Kirchner, J.W., 2017. Debates—Hypothesis testing in hydrology: Theory and practice. Water Resour. Res. 53 (3), 1792–1798. https://doi.org/10.1002/2016WR020116.
Quichimbo, P., Tenorio, G., Borja, P., Cárdenas, I., Crespo, P., Célleri, R., 2012. Efectos sobre las propiedades físicas y químicas de los suelos por el cambio de la cobertura vegetal y uso del suelo: páramo de Quimsacocha al sur del Ecuador. Suelos Ecuatoriales 42 (2), 138–153.
Ramón, J., Correa, A., Timbe, E., Mosquera, G.M., Mora, E., Crespo, P., 2021. Do mixing models with different input requirement yield similar streamflow source contributions? Case study: A tropical montane catchment. Hydrol. Process. 35 (6) https://doi.org/10.1002/hyp.14209.
Regier, P., Briceño, H., Jaffé, R., 2016. Long-term environmental drivers of DOC fluxes: Linkages between management, hydrology and climate in a subtropical coastal estuary. Estuar. Coast. Shelf Sci. 182, 112–122. https://doi.org/10.1016/j.ecss.2016.09.017.
Reinecke, R., Müller Schmied, H., Trautmann, T., Seaby Andersen, L., Burek, P., Flörke, M., Gosling, S.N., Grillakis, M., Hanasaki, N., Koutroulis, A., Pokhrel, Y., Thiery, W., Wada, Y., Yusuke, S., Döll, P., 2021. Uncertainty of simulated groundwater recharge at different global warming levels: A global-scale multi-model ensemble study. Hydrol. Earth Syst. Sci. 25 (2), 787–810. https://doi.org/10.5194/hess-25-787-2021.
Rempe, D.M., Dietrich, W.E., 2018. Direct observations of rock moisture, a hidden component of the hydrologic cycle. Proc. Natl. Acad. Sci. U. S. A. 115 (11), 2664–2669. https://doi.org/10.1073/pnas.1800141115.
Rosset, T., Binet, S., Antoine, J.M., Lerigoleur, E., Rigal, F., Gandois, L., 2020. Drivers of seasonal- And event-scale DOC dynamics at the outlet of mountainous peatlands revealed by high-frequency monitoring. Biogeosciences 17 (13), 3705–3722. https://doi.org/10.5194/bg-17-3705-2020.
Soulsby, C., Tetzlaff, D., Hrachowitz, M., 2009. Advanced Bash-Scripting Guide An in-depth exploration of the art of shell scripting Table of Contents. Hydrol. Process. 23, 3503–3507. https://doi.org/10.1002/hyp.
Staudinger, M., Stoelzle, M., Seeger, S., Seibert, J., Weiler, M., Stahl, K., 2017. Catchment water storage variation with elevation. Hydrol. Process. 31 (11), 2000–2015. https://doi.org/10.1002/hyp.11158.
Tunaley, C., Tetzlaff, D., Soulsby, C., 2017. Scaling effects of riparian peatlands on stable isotopes in runoff and DOC. J. Hydrol. 220–235. https://doi.org/10.1016/j.jhydrol.2017.03.056.
United States Bureau of Reclamation. 2001. Water Measurement Manual: A Guide to Effective Water Measurement Practices for Better Water Management. *Technical Report, Water Resources Research Laboratory, US Department of the Interior*, 317. https://www.usbr.gov/pmts/hydraulics_lab/pubs/wmm/index.htm.
van Huijgevoort, M.H.J., Tetzlaff, D., Sutanudjaja, E.H., Soulsby, C., 2016. Using high resolution tracer data to constrain water storage, flux and age estimates in a spatially distributed rainfall-runoff model. Hydrol. Process. 30 (25), 4761–4778. https://doi.org/10.1002/hyp.10902.
Vázquez, R., 2010. Modelación hidrológica de una microcuenca Altoandina ubicada en el Austro Ecuatoriano. Maskana 1 (1), 79–90.
Veldkamp, T.I.E., Zhao, F., Ward, P.J., de Moel, H., Aerts, J.C.J.H., Schmied, H.M., Portmann, F.T., Masaki, Y., Pokhrel, Y., Liu, X., Satoh, Y., Gerten, D., Gosling, S.N., Zaherpour, J., Wada, Y., 2018. Human impact parameterizations in global hydrological models improve estimates of monthly discharges and hydrological extremes: A multi-model validation study. Environ. Res. Lett. 13 (5), 055008. https://doi.org/10.1088/1748-9326/aab96f.
Viviroli, D., Dürr, H.H., Messerli, B., Meybeck, M., Weingartner, R., 2007. Mountains of the world, water towers for humanity: Typology, mapping, and global significance. Water Resour. Res. 43 (7) https://doi.org/10.1029/2006WR005653.

Vuille, M., 2013. Climate Change and Water Resources in the Tropical Andes. IDB Technical Note 515, 29. http://link.springer.com/article/10.1007/s00382-014-2114-8.

Vuille, M., Bradley, R.S., Keimig, F., 2000. Climate variability in the Andes of Ecuador and its relation to tropical Pacific and Atlantic Sea surface temperature anomalies. J. Clim. 13 (14), 2520–2535. https://doi.org/10.1175/1520-0442(2000)013<2520:CVITAO>2.0.CO;2.

Wang, Q., Wang, L., Huang, W., Wang, Z., Liu, S., Savić, D.A., 2019. Parameterization of NSGA-II for the optimal design of water distribution systems. Water (Switzerland) 11 (5). https://doi.org/10.3390/w11050971.

Wei, X., Hayes, D.J., Fernandez, I., Zhao, J., Fraver, S., Chan, C., Diao, J., 2021. Identifying key environmental factors explaining temporal patterns of DOC export from watersheds in the conterminous United States. J. Geophys. Res. Biogeo. 126 (5).

Werner, B.J., Musolff, A., Lechtenfeld, O.J., De Rooij, G.H., Oosterwoud, M.R., Fleckenstein, J.H., 2019. High-frequency measurements explain quantity and quality of dissolved organic carbon mobilization in a headwater catchment. Biogeosciences 16 (22), 4497–4516. https://doi.org/10.5194/bg-16-4497-2019.

Zhiña, D.X., Mosquera, G.M., Esquivel-Hernández, G., Córdova, M., Sánchez-Murillo, R., Orellana-Alvear, J., Crespo, P., 2022. Hydrometeorological factors controlling the stable isotopic composition of precipitation in the tropical alpine highlands of south Ecuador. J. Hydrometeorol. 76 https://doi.org/10.1175/JHM-D-21-0180.1.

Zitzler, E., Thiele, L., Laumanns, M., Fonseca, C.M., Da Fonseca, V.G., 2003. Performance assessment of multiobjective optimizers: An analysis and review. IEEE Trans. Evol. Comput. 7 (2), 117–132. https://doi.org/10.1109/TEVC.2003.810758.